

# Integrated Geological and Geophysical Mapping for Groundwater Potential Studies at Ekwegbe-Agu and Environs, Enugu State, Nigeria

Charles Chibueze Ugbor\*, Ugochukwu Kingsley Ogbodo, Osita Kenechi Eze

Department of Geology, University of Nigeria, Nsukka, Nigeria

Email: \*charles.ugbor@unn.edu.ng

**How to cite this paper:** Ugbor, C.C., Ogbodo, U.K. and Eze, O.K. (2024) Integrated Geological and Geophysical Mapping for Groundwater Potential Studies at Ekwegbe-Agu and Environs, Enugu State, Nigeria. *Open Journal of Geology*, 14, 513-547. <https://doi.org/10.4236/ojg.2024.144021>

**Received:** November 19, 2023

**Accepted:** March 15, 2024

**Published:** April 18, 2024

Copyright © 2024 by author(s) and Scientific Research Publishing Inc. This work is licensed under the Creative Commons Attribution International License (CC BY 4.0).

<http://creativecommons.org/licenses/by/4.0/>



Open Access

## Abstract

The study integrates both the geological and geophysical mapping techniques for groundwater potential studies at Ekwegbe-Agu and the environs, Enugu state, Nigeria for optimal citing of borehole. Located in the Anambra Basin between latitudes 6°43'N and 6°47'N and longitudes 7°28'E and 7°32'E, it is stratigraphically underlain by, from bottom to top, the Enugu/Nkporo, Mamu and Ajali Formation respectively, a complex geology that make citing of productive borehole in the area problematic leading to borehole failure and dry holes due to inadequate sampling. The study adopted a field and analytic sampling approach, integrating field geological, electrical resistivity and self-potential methods. The software, SedLog v3.1, InterpexIx1Dv.3, and Surfer v10 were employed for the data integration and interpretation. The result of the geological field and borehole data shows 11 sedimentary facies consisting of sandstone, shales and heterolith of sandstone/shale, with the aquifer zone mostly prevalent in the more porous sand-dominated horizons. Mostly the AK and HK were the dominant curve types. An average of 6 geo-electric layers were delineated across all transects with resistivity values ranging from 25.42 - 105.85  $\Omega$ m, 186.38 - 3383.3  $\Omega$ m, and 2992 - 6286.4  $\Omega$ m in the Enugu, Mamu and Ajali Formations respectively. The resistivity of the main aquifer layer ranges from 1 to 500  $\Omega$ m. The aquifer thickness within the study area varies between 95 and 140 m. The western and northwestern part of the study area which is underlain mainly by the Ajali Formation showed the highest groundwater potential in the area and suitable for citing productive boreholes.

## Keywords

Seismic, Ekwegbe-Agu, Groundwater, Resistivity, Field Mapping, Borehole

## 1. Introduction

Groundwater is water that exists under the Earth's surface and fills all or part of the void spaces in soils or geologic strata. Groundwater is sometimes known as subsurface water to differentiate it from surface water, which is found in enormous bodies of water such as the seas or lakes or flows overland in streams. Groundwater is the biggest reserve of potable water and one of the most important sources of supply in areas where people live, it is of critical importance to modern society. This groundwater may appear at the surface in the form of springs, and it can also be extracted through wells.

It is an integral component of the natural hydrologic cycle, constituting the majority of the cycle [1]. Groundwater can be found in a variety of geological formations and occurs in aquifers, which are porous geological formations that can store and transmit water [2]. Recent developments have been employed to characterize the nature and the pattern of flow of groundwater which generally categorized groundwater into groundwater found in the unsaturated zone and groundwater located in the saturated zone [2]. This categorization is due to the differences in the physics of water flow in saturated and unsaturated zones and to comprehend these, the distribution of geological materials with differing hydraulic conductivity and porosity is essential [3]. In groundwater potential studies, the knowledge of the geology of the area under investigation is very crucial as the understanding of the geology of the site helps to delineate possible saturated zones from unsaturated zones beneath the crust and this helps in the exploration of groundwater [4]. The Exploration of groundwater is of the utmost significance because homes and businesses require water for a variety of essential functions, including cooking, drinking, and construction purposes. Exploration of groundwater can be carried out using a variety of geophysical techniques ranging from electrical, seismic, and electromagnetic methods [5], however, the electrical resistivity technique appears to be the most commonly utilized method in groundwater studies. The resistivity method of geophysical investigation is used to determine the lateral and/or vertical variation in electrical properties (in this case, resistance or conductivity) of sub-surface rock materials that serve as conduits for groundwater resources [5]. Hence, it can be used to spot or identify porous zones or areas in the sub-surface that possess high potential for groundwater resources based on the values of measured apparent resistivity which is dependent on the amount of injected current, the potential difference recorded and the electrode configuration employed [3]. Groundwater potential is a function of complex inter-relationship between, geology, physiography, groundwater flow pattern, recharge and discharge processes [3]. However, the use of relationships and comparisons between aquifer properties, hydrogeological and ge-

ophysical parameters [6], has also proved useful for groundwater potential modelling.

The Ekwgbe-Agu and its environs have begun to witness an upsurge in infrastructural development ranging from Maduka University to estates and businesses. This has led to an increase in human population in the area, which is expected to double soon as a result of urbanization. Hence, the demand for portable water for human consumption, industrial, and agricultural purposes will likely grow astronomically and with the present supply grossly inadequate and cases of abortive boreholes of extremely low yields as well as a total failure of some supply wells in the area, there is a need for detailed groundwater study in the area to identify sites for drilling productive boreholes within the Ekwgbe-Agu and environs to ensure a portable and sufficient amount of water that will adequately serve the populace in the near future.

To achieve this, the integration of geophysical methods with borehole data becomes essential; the electrical resistivity technique when integrated with borehole and geological a-priori data has proven to be very successful. [7] employed the resistivity technique (Vertical electrical sounding) and geophysical logs to map and characterize aquifer units in a typical complex transition zone of Ijebu Ode in Ogun state, Nigeria. [8] and [9] used resistivity data and overburden thickness to evaluate the groundwater potential in a basement complex terrain. Also, [10] utilized resistivity data and local geology to evaluate the groundwater potential in a deltaic plain deposit. Furthermore, researchers such as [11] [12] and [13] also used the resistivity method in their studies within the Ajali Formation, however, the identification of aquitard units within the formation by [14] and failure of boreholes in some of the area prompted the use of SP logs to validate the results from the resistivity technique. [15] investigated the groundwater occurrence at Obollo Affor, southeastern Nigeria using integrated geophysical methods, essentially electrical resistivity and Self-potential (SP) well log and got a highly confident result as the borehole (SP log) helped to identify the saturated zone despite the presence of some clay beds which had resistivity values close to that of water. [16] also undertook a study of the groundwater at the Enugu metropolis and the environs, in southeast Nigeria using resistivity sounding in combination with aeromagnetic data and were able to isolate aquifer-bearing locations in the area.

Hence this study aims to integrate geological, borehole and ground geophysical data to investigate the sub-surface geological formations for groundwater resources to identify areas that are most suitable for citing productive boreholes within Ekwgbe-Agu and the environs, Enugu state, Nigeria. This research is expected to provide the solution to the random failure of boreholes in the area due to complex geology and inadequate understanding of the aquifer distribution/layers in the area prior to the study. The study area is receiving increased in human activity, especially development from the citing of new University in the area. Currently citing of borehole in the area has become a big challenge with multiple failures of due to dry holes arising from poor understanding of the ge-

ology and hydrogeology status of the area. This research thus tries to illuminate the hydrogeological conditions and to highlight the regions that will be prolific and exclude regions that are unlikely to result in dry holes using integrated study of both hydrological and geophysical characteristics. The result of this study will thus serve as guide to the public in deciding where to cite the boreholes for both private and public use. **Figure 1** shows the location map of the study area, Ekwegbe, Opi and the environs, showing the accessibility.

## **1.1. Geology of the Study Area**

### **1.1.1. Regional Stratigraphic Setting**

The study area lies within the Anambra Basin. The basin is a NE-SW trending syncline that is part of the Central African Rift System which developed in response to the stretching and subsidence of major crustal blocks during a Lower Cretaceous break-up phase of the Gondwana super-continent [17]. It's the oldest sedimentary basin in Nigeria and originated in the early Cretaceous as the failed rift associated with the opening of the South Atlantic [18]. The Benue Trough, which forms a part of the Central West African Rift System of Niger, Chad and Sudan, in Nigeria consists of a series of rift basins. The period of subsidence in southern Benue Trough corresponds to the time of the initiation of the Anambra Basin, which started during the Coniacian and reached its peak at the Santonian thermo-tectonic event [19].

The Anambra Basin is a synclinorium with a horseshoe configuration, with its apex bounding against the Makurdi sub-basin on the east and southeast by the Abakaliki Basin. It opens southwestwards into the Niger Delta Basin. The Proto-Anambra Basin was a platform that eventually became thin sediment-draped at the time the Abakaliki-Benue sector of the Benue Trough was being filled which occurred during Albion-Santonian [20]. Deposition eventually became very slow or ceased altogether as a result of the regression of the sea, and the sediments were strongly folded. In Turonian time, the sea again invaded large areas, and marine sedimentation continued well into Santonian. This was followed by uplift and renewed folding, and erosion in certain areas. In Campanian-Maastrichtian times, another transgression of the sea took place and marine sediments were laid down. In some areas, these rests unconformably on the underlying beds, while in others there appears to have been no break in sedimentation.

The sea slowly regressed towards the close of Maastrichtian; this led to the formation of an extensive, low-lying coastal area with lagoons and swamps, on which a thick succession of coal measures formed. Fresh-water sandstones were deposited, extending to the north and west onto the Precambrian basement. Sedimentation was entirely non-marine until the deposition of the Upper Coal Measures, in which marine intercalations indicate a gradual encroachment of the sea. Sedimentation was again marine during the Palaeocene and lower Eocene, but during Miocene time there was widespread emergence of the coastline, with the re-establishment of conditions favourable for the deposition of freshwater

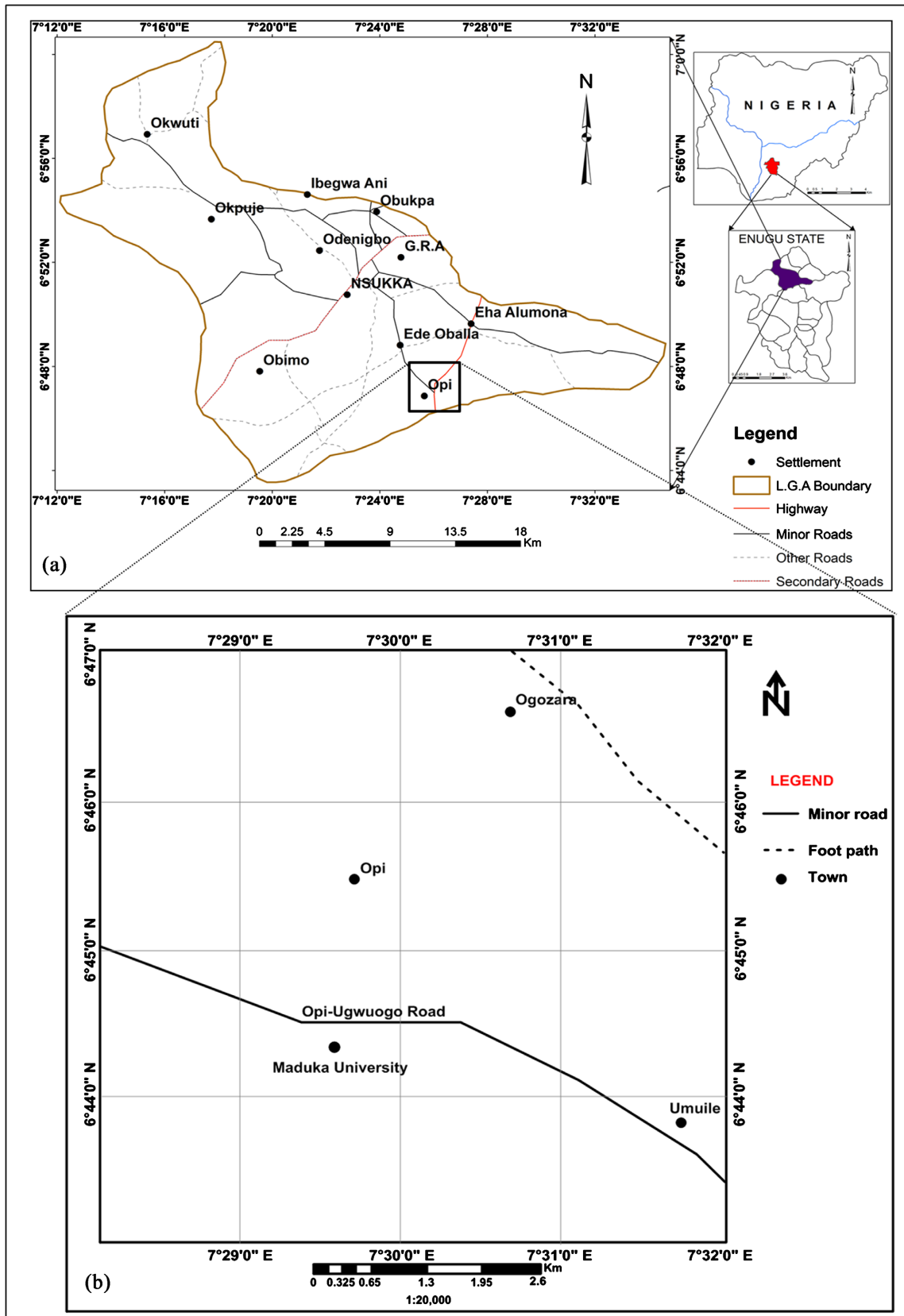


**Figure 1.** Location map of the study area in the Anambra Basin: (a) Inset map of Nigeria, showing the location of Ekwegbe/Opi in map of Enugu state. (b) Accessibility map of the study area.

sediments, carbonaceous beds and lignite. The various lithostratigraphic units that make up the Anambra Basin include the Nkporo Group, Enugu Shale, Mamu Formation, Ajali Sandstone and Nsukka Formatio [21]. **Figure 2** shows the stratigraphic succession of the Cretaceous-Recent sediments in southeastern Nigeria underlying the Abakaliki Basin, Ikom-Mamfe Embayment (IME), Anambra Basin and Niger Delta Basin

**1.1.2. Local Geology**

The study area lies in the Anambra basin and is underlain from bottom to top by three prominent geologic Formations; Enugu Formation, Mamu Formation and Ajali Formation respectively. The Enugu Formation is made up of carbonaceous shales with the upper half deposited in a lower floodplain and swampy environments and overlies the Nkporo Group [22]. The Mamu Formation, which used

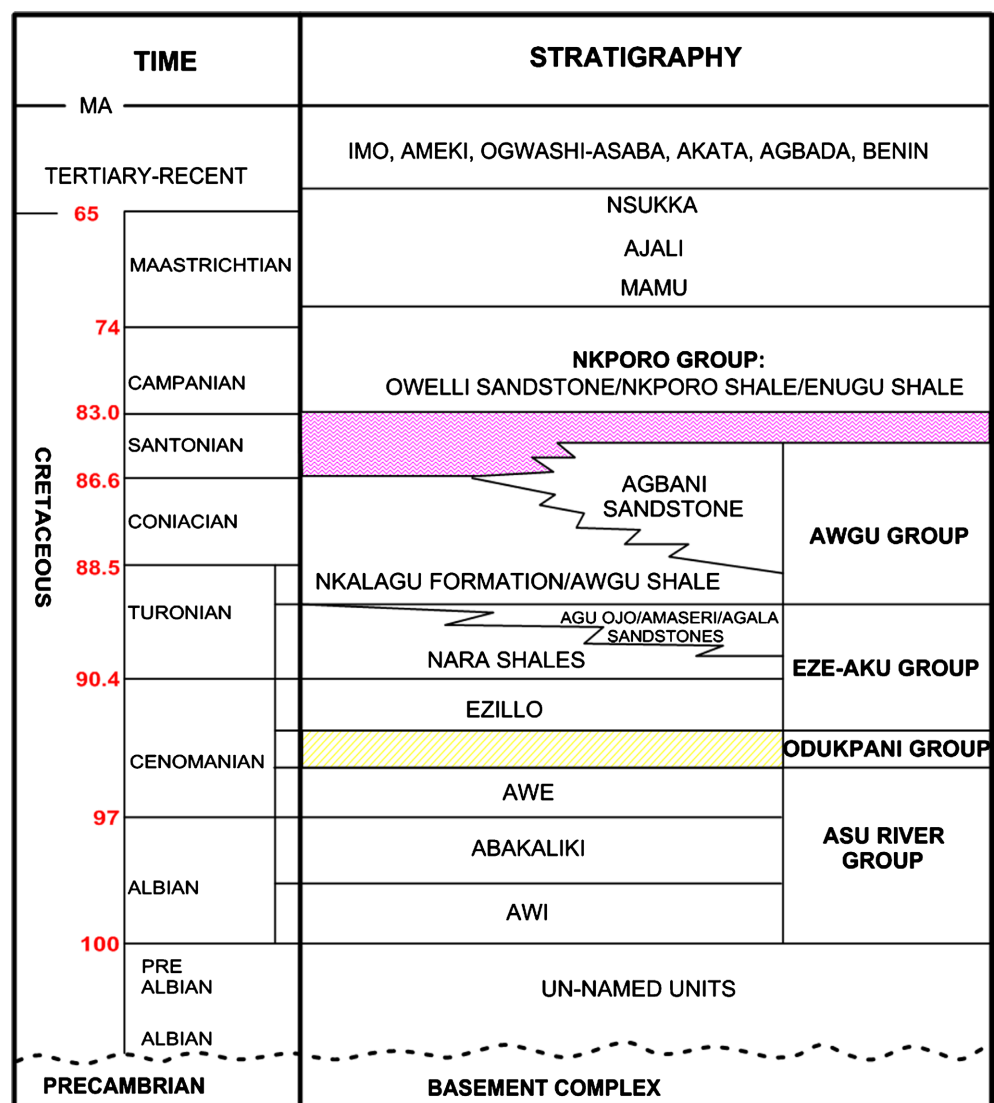


**Figure 2.** Stratigraphic succession of the Cretaceous-Recent sediments in southeastern Nigeria underlying the Abakaliki Basin, Ikom-Mamfe Embayment (IME), Anambra Basin and Niger Delta Basin (redrawn after [20]).

to be called the Lower Coal Measures, has marine intercalations made of ammonite-containing shales [23] and [24] noted that the sediment pile varies across the Anambra basin and ranges from 75 to over 1000 meters in different parts of the basin. The lithology of the Mamu Formation varies from fine-medium-grained, white to grey sandstones, shaly sandstones, sandy shales, grey mudstones, shales and coal seams [25]. The fine-grained sandstone unit of the Mamu Formation provides the shaly impermeable base on which the aquifer in the Ajali Formation is laid. The Ajali Formation overlies the Mamu Formation and it is often referred to as the “False-Bedded Sandstone” [26] and the type locality is in the valley of the Ajali River near Enugu [27]. The Ajali formation is mostly loose, poorly sorted, coarse-to-fine-grained, poorly cemented sandstone, mudstone, and siltstone, and it dates from the middle to late Maastrichtian. Ajali Formation is found within the study area and it is covered by a thick layer of red earthy sands that were formed by weathering and ferruginization. The thickness of this layer varies from less than 300 meters to more than 1000 meters in the middle of the basin [27] [19]. Cross-bedded sedimentary structures are commonly observed on the sands of the Ajali Formation within the study area. These structures are encountered near reactivation surfaces, mud drapes, tidal bundles, backflow ripple channels cut and lateral accretion surfaces [22].

## **2. Materials and Method of Study**

### **2.1. Materials**

The materials used for this study include the Abem Terrameter used for acquiring geophysical data, field geological mapping tools: topo map, compass, Global Positioning System (GPS) device, and geological hammer. Geophysical logs: Resistivity and self-potential logs, Analytical tools include ArcGIS and Win Resist.

### **2.2. Method of Study**

The method adopted includes field geological mapping, a Geophysical survey using the resistivity method and well logs obtained from wells. These data were integrated for interpretation of the subsurface.

The following detail about each method is presented.

#### **2.2.1. Field Geological Studies**

Extensive geological field studies were carried out in the study area which involved systematic vertical and lateral description of the arrangement of lithologies and their variability in terms of strata thickness, orientation, texture, and composition. The results were plotted using the SedLog Software and displayed as lithologic sections. The thickness of the beds is displayed in meters on the various lithologic sections and measurements of the attitudes of beds were recorded and indicated on maps. The geographic coordinates of each outcrop location were recorded with a Garmin Global Positioning System (GPS). The GPS coordinates were later transferred onto a Minna geodetic datum georeferenced base map of Ogozara-Opi and environs using the MapInfo Geographical Infor-

mation System (GIS) platform.

### 2.2.2. Geophysical Investigation

Borehole logging and electrical resistivity methods of geophysical surveying were conducted in selected locations of the study area. The results of field descriptions were employed in the interpretation of geophysical measurements, particularly in the calibration of vertical electrical sounding data.

### 2.2.3. Borehole Logging

Geophysical borehole logging, also known as downhole geophysical surveying or wire-line logging, is used to derive further information about the sequence of rocks penetrated by a borehole [28]. Geophysical borehole logging can define the depth to geological interfaces or beds that have a characteristic geophysical signature, to provide a means of correlating geological information between boreholes and to obtain information on the in situ properties of the wall rock. The instrumentation necessary for borehole logging is housed in a cylindrical metal tube known as a sonde. Sondes are suspended in the borehole from an armoured multicore cable. They are lowered to the base of the section of the hole to be logged, and logging is carried out as the sonde is winched back up through the section. The surface instrumentation, including recorders, cable drums and winches, is usually installed in a special recording truck located near the well-head. Spontaneous Polarization (SP) data was taken to identify the boundaries between shale horizons and more porous beds as well as their correlation between boreholes. **Figure 3(a)** is an illustration of a typical SP tool and illustration as a reliable tool in the application as a lithology discriminator. In operation, the

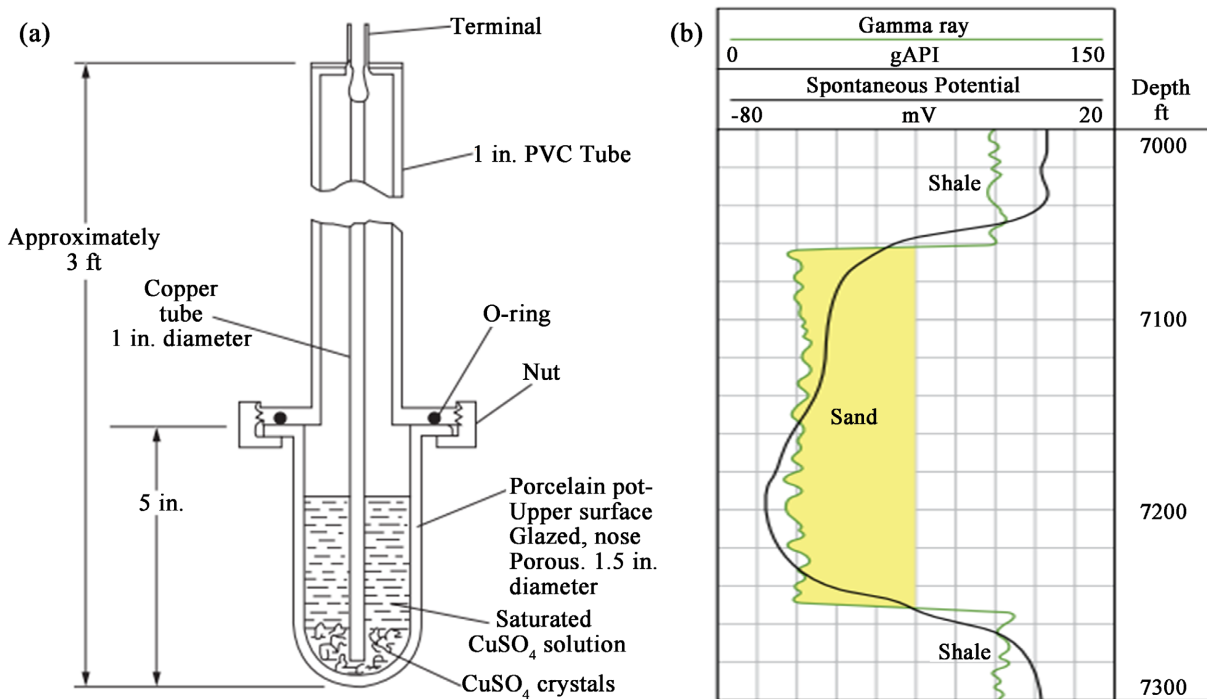


**Figure 3.** (a) Illustration of surface tool for SP method (b) Typical SP response as a lithology discriminator [30].

sode is lowered into the borehole while one end of the terminal is fixed on the surface. The electrical pulse is passed through the cable down the hole, while the Self Potential is read off the digital display. The depth of probe is increased at regular interval and logged successively at each SP measurement till the end of the test hole. A typical log of the SP measurement is shown in **Figure 3(b)** where it is used to discriminate between sandstone and shale lithology. The essence of combining the SP logging with the resistivity measurement in the area is to be able to isolate the sand packages in the area that are target for ground water accumulation. This becomes necessary since the area is underlain by thick sequences of shales. These shales most times show similar low resistivity values especially when wet, which could misrepresent the layer as an aquifer. The use of SP log here therefore eliminates this ambiguity.

In the current study, two borehole data (BH 1, and BH 2) respectively were acquired and analyzed to show the various stratigraphic units that underlie the study area along with their thicknesses, resistivities and self-potential values. These data were used to calibrate sounding curves obtained from surface resistivity measurements. The locations of the sampling points are shown in **Figure 4**.

#### **2.2.4. Electrical Resistivity Method**

The Vertical electrical sounding (VES) technique which is known to have superior vertical sensitivity [30] was adopted to determine the depth variation in apparent resistivity. The potential electrodes were stationary along the traverse while the current electrodes were symmetrically expanded about a fixed central point and readings indicating vertical thickness variations were taken at discrete locations along the profile using the Omega resistivity meter.

However, for very large current electrode separation, the electro-potential distance was increased to maintain a measurable potential. A total of nineteen (19) VES were taken within the study area. Of these, eight (8), ten (10) and one (1) VES station, respectively, were run within the Ajali, Mamu and Enugu formations in the study area. The VES stations are well distributed within the entire area. The underlying stratigraphy for all VES point located within each formation and the summary of the aquifer geo-electric parameters is presented in **Table 1**.

Data obtained from the VES stations were imported into Interpex software and the parameters, resistivity, thickness and depth, of a geo-electric model, thought to be closer to reality (sub-surface resemblance) were estimated, substituted in the aforementioned computer program, edited by trial and error until a very close match was attained between the calculated and observed resistivity. The exported curves were displayed on a log-log paper in terms of distance and depth and the range of resistivity values after graduation was used to mark distinct stratigraphic layers in each transect. These stratigraphic curves were interpreted quantitatively to determine the nature of the underlying geological formations, presented with their possible geological meanings, resistivity values and

**Table 1.** Aquifer geo-electric layer parameters obtained from the VES models (ND: No Data).

VES No.	Northing	Easting	Curve Type	No. of Geo-Electric Layers	Water Table (m) (Approx.)	Aquifer Thickness (m) (Approx.)	Aquifer Resistivity ( $\Omega$ m)
1	6°44'47.26"N	7°29'30.22"E	AK	6	31	58	202.860
2	6°45'12.02"N	7°29'28.52"E	AK	6	22	85	110.050
3	6°45'13.16"N	7°28'14.41"E	HK	6	38	37	113.340
4	6°46'12.42"N	7°29'18.21"E	HK	6	30	133	1163.100
5	6°44'14.18"N	7°28'47.24"E	HK	6	13	42	56.079
6	6°44'30.09"N	7°28'09.43"E	HKA	6	35	60	129.420
7	6°44'28.32"N	7°29'50.89"E	QK	7	33	45	94.276
8	6°44'30.29"N	7°30'43.23"E	HK	6	14	68	429.730
9	6°45'23.01"N	7°30'45.03"E	KHQ	6	82	126	141.910
10	6°45'27.09"N	7°31'35.47"E	KHQ	7	81	79	51.475
11	6°45'15.34"N	7°29'50.29"E	K	6	74	57	78.777
12	6°45'57.26"N	7°29'0.16"E	KA	6	26	31	33.174
13	6°44'40.11"N	7°31'16.14"E	K	6	123	81	205.120
14	6°46'34.48"N	7°24'26.20"E	HKA	6	36	59	77.553
15	6°43'56.20"N	7°30'36.12"E	AK	4	208	ND	7351.900
16	6°45'27.24"N	7°28'20.09"E	AK	4	136	ND	2216.200
17	6°45'21.14"N	7°28'58.36"E	AK	4	136	ND	64.091
18	6°45'52.41"N	7°28'18.21"E	H	6	204	ND	33.884
19	6°43'01.39"N	7°30'35.06"E	H	6	123	81	45.667

layer thicknesses. **Figure 4** shows the geologic map of the study area with the VES profile lines, and the borehole locations where the SP data were acquired.

### 3. Results and Discussion

#### 3.1. Geological Outcrop Analysis

Geological field studies of outcrops within the study area led to the identification of eleven sedimentary facies. These facies were distinguished on a purely descriptive basis and were integrated with borehole data for the calibration of vertical electrical sounding models. The majority of outcrops were encountered within Opi and Uhere-Opi as road-cut sections (**Figure 5** and **Figure 6**) and river sections (**Figure 7**), others were seen exposed at active quarry sites (**Figure 8**). The sedimentary facies observed at outcrop locations include parallel laminated shale facies (Shl), dark grey shale facies (Shgd), light grey shale facies (Shgl), silty sandstone facies (Sst), siltstone facies (St), indurated sandstone facies (Ssi), medium to coarse sandstone facies (Scm), heterolithic facies (Ht), fine-grained sandstone

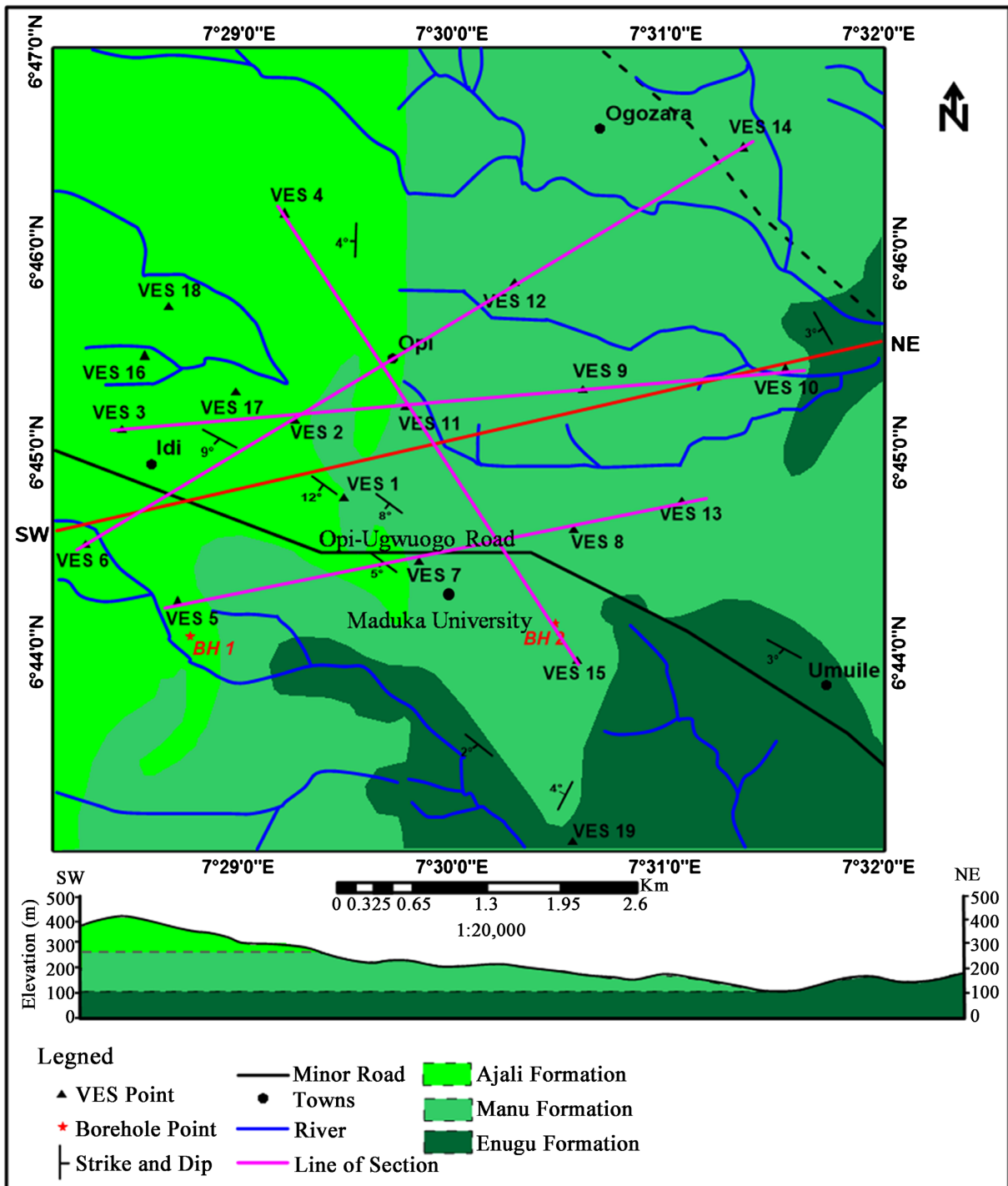


**Figure 4.** Geological map and cross section showing the 3 formations, Ajali, Mamu and Enugu Formations and the Profile lines for acquisition of the geophysical (VES) data and Borehole locations BH1 and BH2 where the SP logs were obtained.

facies (Ssf), medium-grained sandstone facies (Ssm) and claystone (Cl). The letters S, Sh, St, and Cl indicate the dominant grain size and/or lithology: sand, shale and silt, respectively. The lowercase letters l, g, d, i, f, and m are mnemonics for the characteristic texture or structure or both of the facies (lamination, grey, dark, induration, fine, medium), respectively.

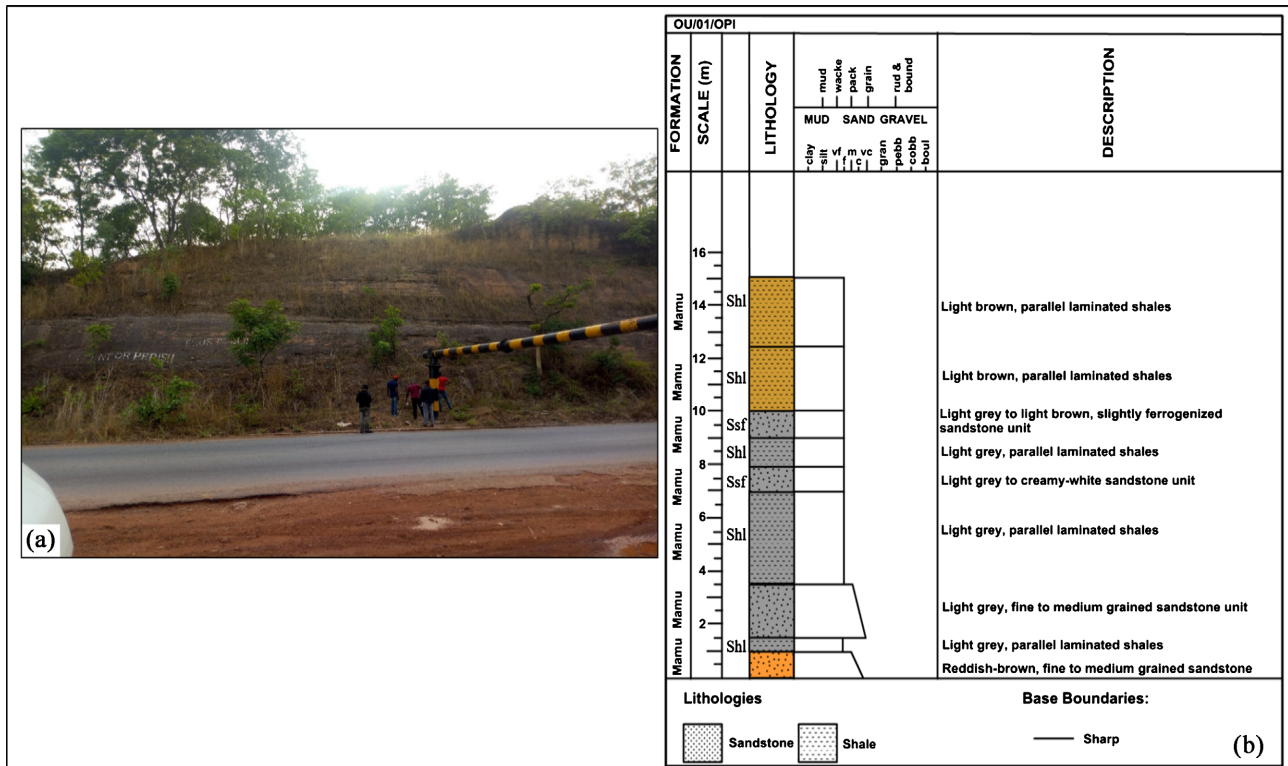


**Figure 5.** (a) A road cut section showing an alternating sequence of shales and sandstone facies encountered along Enugu-Nsukka road (Scale: Human with red cap = 2.40 m) (b) Stratigraphic profile of the outcrop section showing the description of each lithologic unit at Location OU/01/OPI.

Eleven facies were recognized from the sediments of the Ajali and Mamu formations that are exposed in the study area. The analysis of these facies (along with borehole information) provided a platform for assigning lithology to geo-electric layers observed on 1-D electro-stratigraphic models.

The parallel laminated shale facies (Shl) are comprised mainly of thick units of light brown to light grey and creamy-white shales. These facies were observed at Opi in locations OU/01/OPI (Figure 5). At OU/01/OPI, they were observed at the upper, middle and basal sections of the outcrop, and alternated with the fine-grained sandstone facies (Ssf). At OU/01/OPI, the shales occupied the top-most unit of the outcrop section (Figure 5). The dark grey shale facies (Shgd) are very poorly exposed within the study area and it was encountered at Opi, in location OU/02/OPI, where it was exposed as a thick shale unit at the upper part of the outcrop section (Figure 6). The silty-sandstone facies (Sst) is characterized by light grey and creamy-white to light yellow and brown silty sandstone units. They are exposed at the lower and upper parts, respectively, of outcrop sections in Opi located at OU/02/OPI (Figure 6). At OU/02/OPI, Sst is underlain and overlain by thin units of light grey shale facies (Shgl) and fine-grained sandstone facies (Ssf), respectively (Figure 6). The light grey shale facies (Shgl) are fairly exposed within the study area. Shgl occurs at the upper and lower parts of the outcrop section seen at location OU/02/OPI, where it has a thickness that ranges from 0.25 to 0.5 m and is underlain by a thick unit of weathered shale

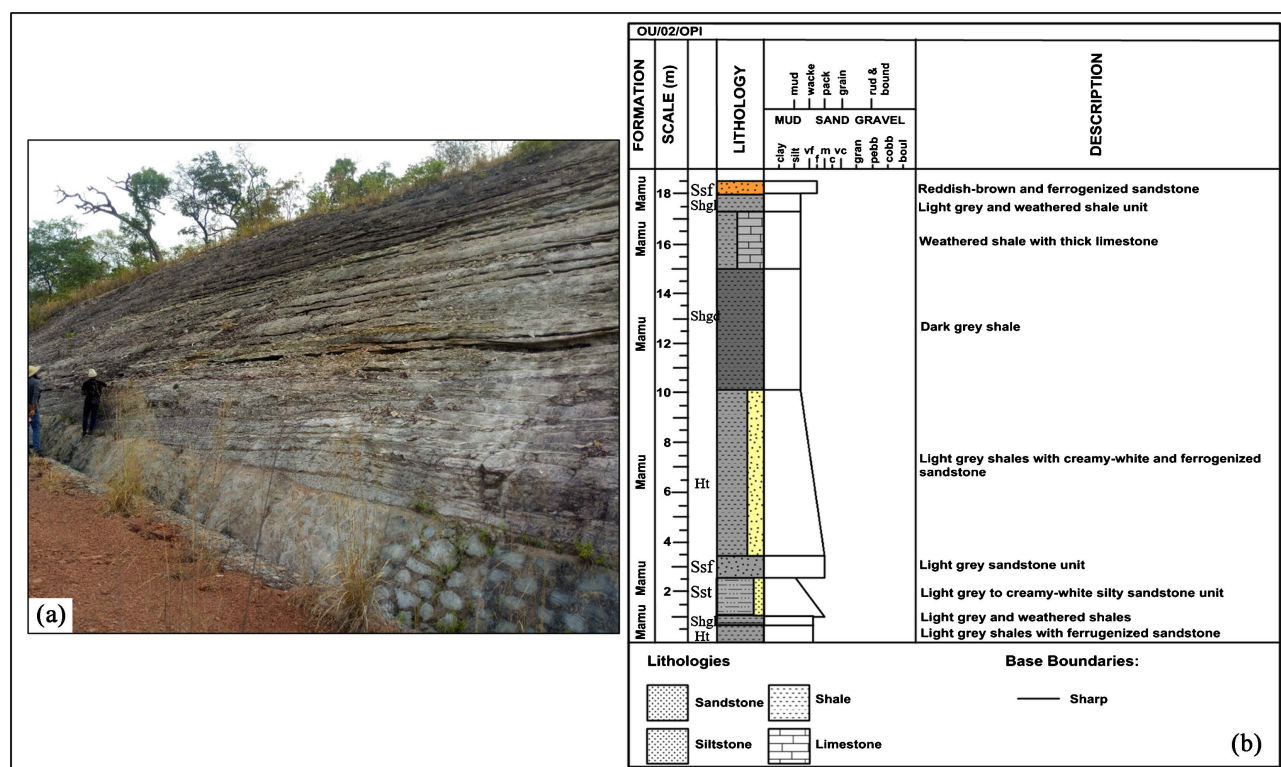


**Figure 6.** (a) Outcrop photograph showing a vertically and laterally extensive unit of sediments observed along the Enugu-Nsukka road, Opi (Scale: Human = 2.85 m) (b) Stratigraphic profile of the logged section showing the thick unit of dark grey shale facies (Shgd) at Location OU/02/OPI.

that is interbedded by a unit of limestone (Figure 6). Siltstone Facies (St) is widespread and pronounced within the study area, it occurs as thick and relatively thick, yellowish to milkfish, light-yellow to brown and sometimes creamy-white coloured siltstone unit. Bed thickness ranges from 1 m to 4 m with sharp contacts at the top and base (Figure 5, and Figure 6). They are mainly observed in Opi, at the middle and lower parts of the outcrop section that occur at locations OU/01/OPI, OU/02/OPI (Figure 5 and Figure 6). The indurated sandstone facies (Ssi) are poorly exposed within the study area, it was observed in one location (OU/01/OPI) at the middle part of the outcrop where it is directly overlain and underlain by the parallel laminated shale facies (Shl) and the siltstone facies (St) (Figure 5). The fine-grained sandstone facies (Ssf) is perhaps the most extensive and pronounced facies encountered within the study area. It is made up of light grey, white to light yellow, creamy-white to reddish-brown and light brown, well sorted and sometimes horizontally laminated and iron stained fine-grained sandstone unit. Specifically, Ssf occurred in locations OU/01/OPI, OU/02/OPI, OU/06/OPI and OU/08/OPI (Figures 5-8). At OU/01/OPI (Figure 5), these facies are overlain and underlain by the parallel laminated shale facies (Shl) whereas, at OU/06/OPI (Figure 7) and OU/08/OPI (Figure 8), it is overlain by the claystone facies (Cl). The white-coloured unit of these facies at the base of the outcrop exposure at OU/06/OPI had clay drapes while the uppermost Ssf at OU/08/OPI was characterized by a thin band of ironstone (Figure 8).

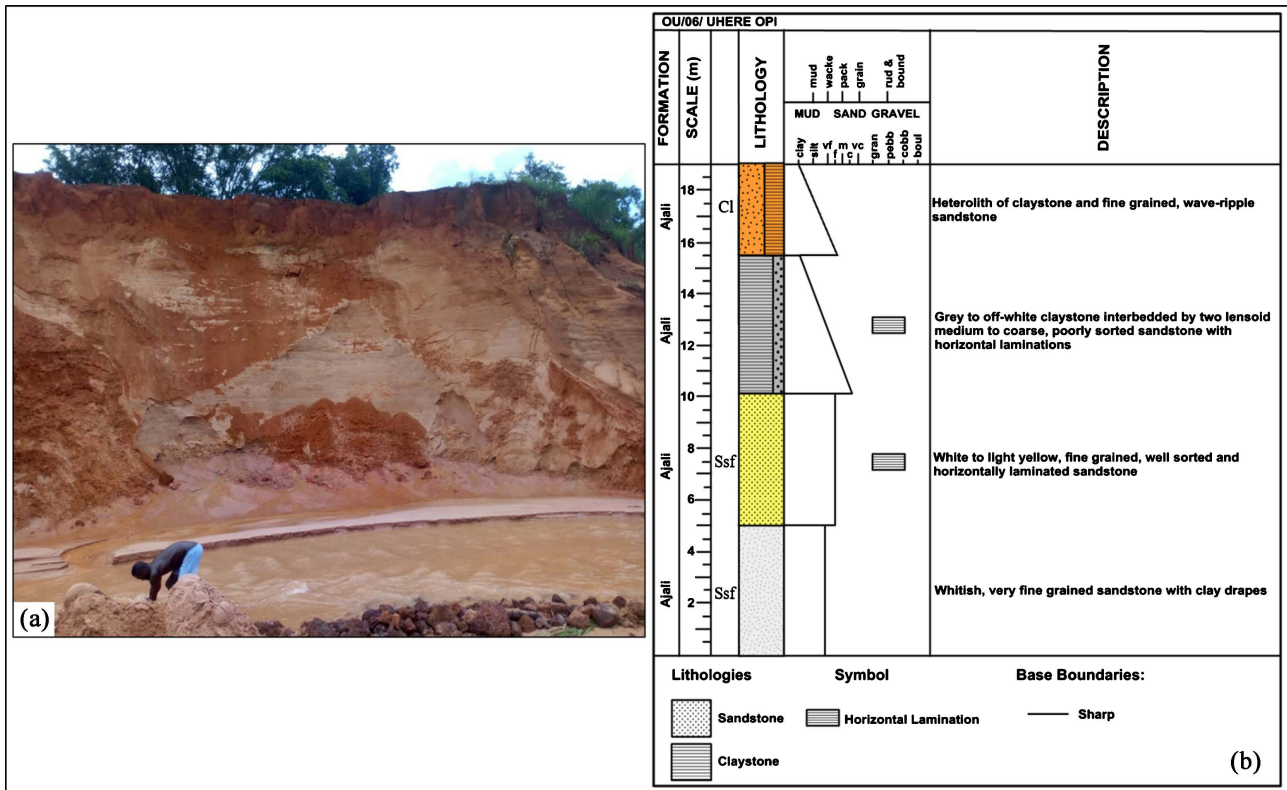


**Figure 7.** (a) A river section showing a thick deposit of friable sands observed at Uhre-Opi (Scale: Squating human in the centre foreground = 2.60 m) (b) Lithologic profile of the outcrop section showing the description of each lithologic unit at Location OU/06/OPI.

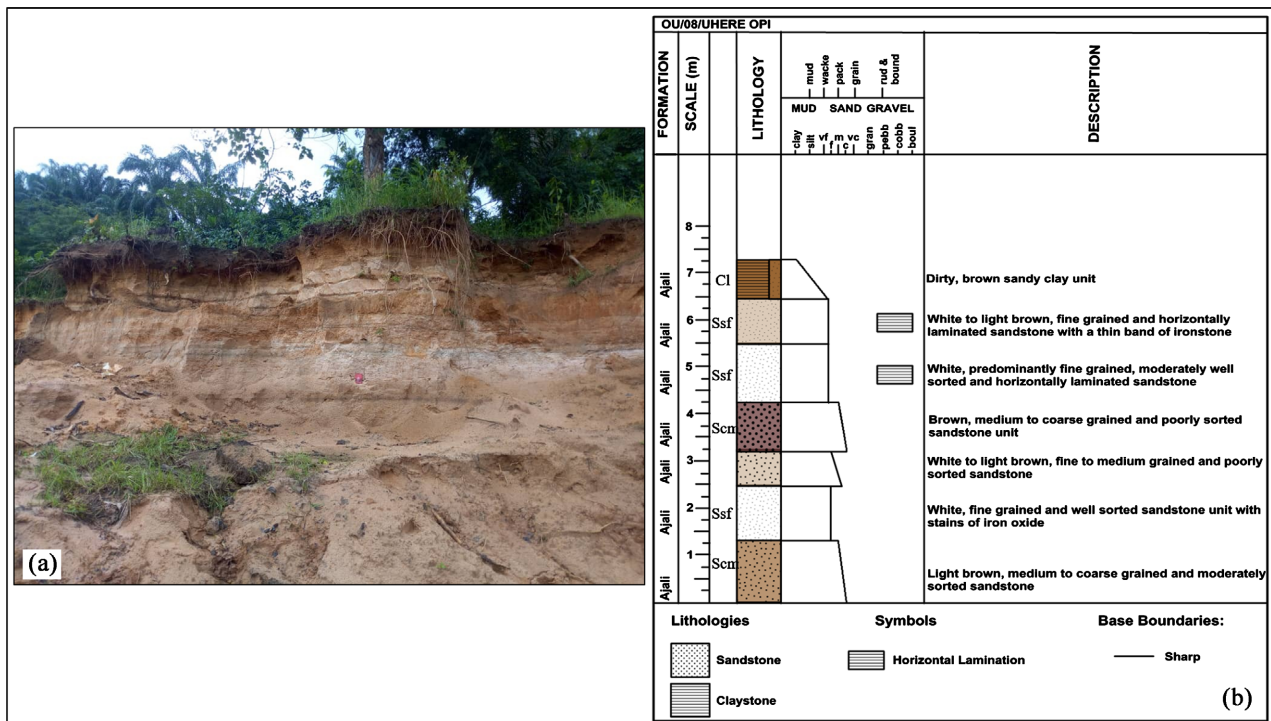


**Figure 8.** (a) Outcrop photograph showing a thick deposit of clay and sand exposed at a section of an active quarry site in Uhre-Opi (Scale: Red field notebook = 5.0 cm) (b) Lithologic profile of the logged section showing the fine-grained sandstone (Ssf) and claystone facies (Cl) at Location OU/08/OPI.

Claystone facies (Cl), observed at Uhere-Opi, mainly consists of reddish-brown to brown, dirty and sometimes horizontally laminated and lateritized claystone units. They are found exposed at the topmost parts of outcrop sections in locations that include OU/06/OPI, and OU/08/OPI (**Figure 7** and **Figure 8**). The heterolithic facies (Ht) are not widespread and occur at the upper, middle and basal parts of outcrop sections in Opi and Uhere-Opi at locations OU/02/OP I (**Figure 6**) and OU/08/OPI (**Figure 8**) (also see **Figure 6**). At OU/02/OPI, Ht was found to be thickly and thinly bedded, respectively, at the middle and basal sections of the outcrop where it is overlain by either the light grey shale facies (Shgl) or the dark grey shale facies (Shgd) (**Figure 6**). The medium to coarse-grained facies (Scm) consists of brown, light brown and/or brown to yellow, moderately to poorly sorted sandstone units (**Figure 7** and **Figure 8**).

### 3.2. Interpretation of Borehole Data

Results of self-potential (SP) and resistivity logging from two boreholes (BH 1 and BH located in the southwestern and southeastern parts of the study area as seen the geologic/location map (**Figure 4**) were analyzed and correlated with the sample cuttings. The obtained results from the short and long-normal resistivity logs display the resistivity values of the geologic formation at shallow and deep intervals, which were penetrated. The natural potential of the penetrated geologic formations to the shale baseline is indicated on the SP log.

BH 1 is sited close to VES 5 and probed a total depth of about 260 m. The uppermost interval, which commences at the point where probing began, and occurs between a depth of 20 and 55 m is the saturated zone. It is characterized by low resistivity values with a corresponding high SP signature. However, the resistivity and SP values appear to gradually increase and decrease, respectively, as logging continued downward (**Figure 9**).

This suggests a gradual reduction in saturation (downwards) within this layer as it approaches the underlying dark grey shales. The depth to the zone of saturation in BH 1 also coincides with the low resistivity water-bearing interval in VES 5. Hence, by a fair approximation, the log data of BH 1 and VES 5 are in agreement and show similar sub-surface conditions. The geophysical signatures indicated by the nearby VES model (VES 5) and BH 1, between a logging depth of 20 and 55 m, show that this borehole could be productive (**Figure 9**). It is, therefore, deducible to recommend that boreholes drilled within this area should be conditioned to a depth of 55 m to ensure maximum water yield.

The underlying zone, which occurs between 55 and 80 m, shows contrasting resistivity and SP readings when compared to the saturated zone. The deflection of the resistivity and SP curves, which indicate high and low values, respectively, supports a dark grey shaly interval that is admixed with siltstone (**Figure 9**). Its geophysical signatures depict features of a non-water bearing zone. Although the SP curve shows a continuous decrease in SP values almost throughout this interval (except at 75 - 80 m where it appears to show the onset of an increase), the

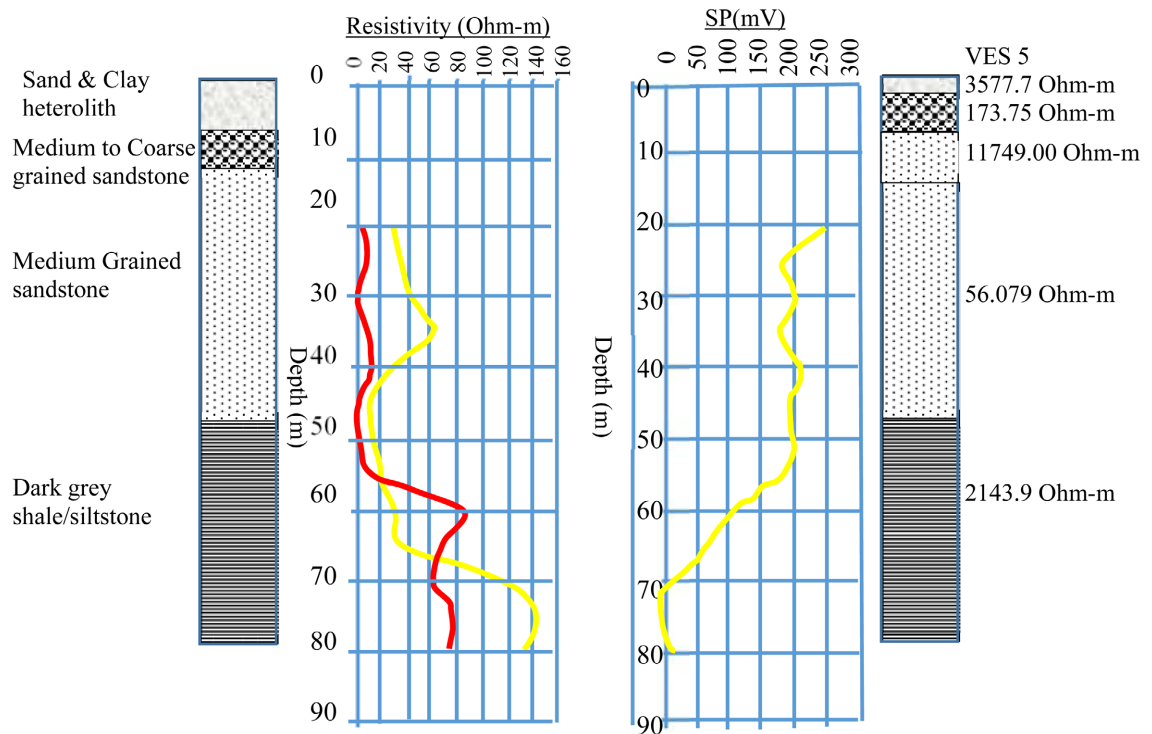


**Figure 9.** Resistivity and self-potential logs of BH 1, its lithological sequence and correlation with VES 5.

resistivity curve (short normal) increases up to about 60 m after which it decreases slightly; an indication that the shallow section of this unit could be wet (as a result of the borehole drilling mud) (**Figure 9**).

BH 2 is located in the southeastern part of the study area and is close to VES 15. Six geo-electric intervals delineated by the sub-surface wireline logs and occurring between a probing depth of about 30 m and 260 m were recognized in this borehole (**Figure 10**).

The first geo-electric zone commences at about 30 m and terminates at about 50 m in the sub-surface. The (long and short normal) resistivity logs and SP curves indicate the presence of wet shales and siltstones. The presence of saturated shallow-seated fractures within the sub-surface could also give rise to the low resistivity and relatively high SP trends observed in these curves.

The second geo-electric interval, which comprises a silty sandstone unit, occurs between a depth of 60 and 75 m. This zone exhibits the characteristics of a water-bearing layer similar to the overlying layer based on the deflection of the resistivity and SP curves. However, the short stratigraphic interval (**Figure 10**) implies that a borehole conditioned to this drilled depth could have a low yield, and thus is not viable for borehole development. The high resistivity (33729  $\Omega$ m) of this zone as indicated by the nearby VES station (VES 15) discourages well-bore development at this depth.

The third geo-electric zone is marked from 75 m to about 110 m in logging depth (**Figure 10**). It also exhibits a relatively low SP trend. The lesser resistivity trend of the long normal resistivity log with the corresponding relatively high SP

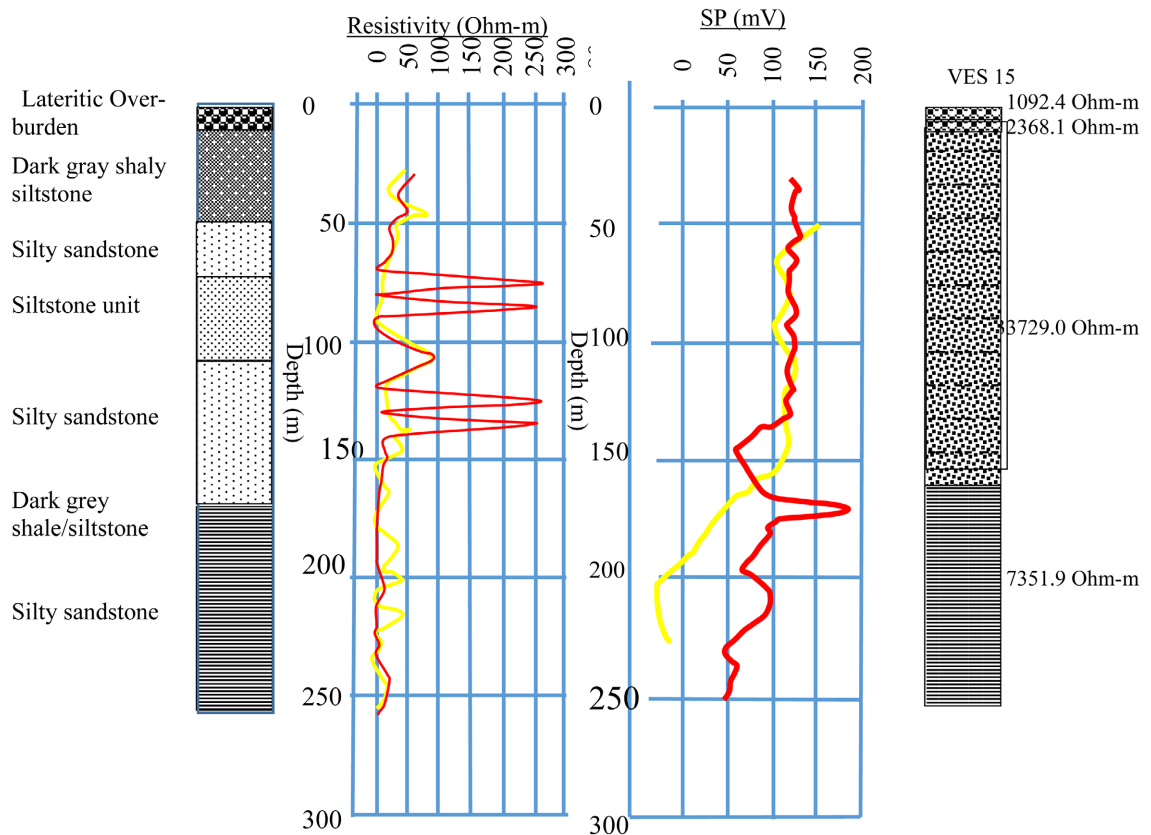


**Figure 10.** Resistivity and self-potential logs of BH 2, its lithological sequence and correlation with VES 15.

indicates that the deeper sections of this siltstone zone are saturated and could be viable for borehole installation. On the other hand, the short normal resistivity log displays a fluctuating high and low trend, which suggests that part of the shallow sections of the siltstone interval have been invaded by drilling mud (**Figure 10**).

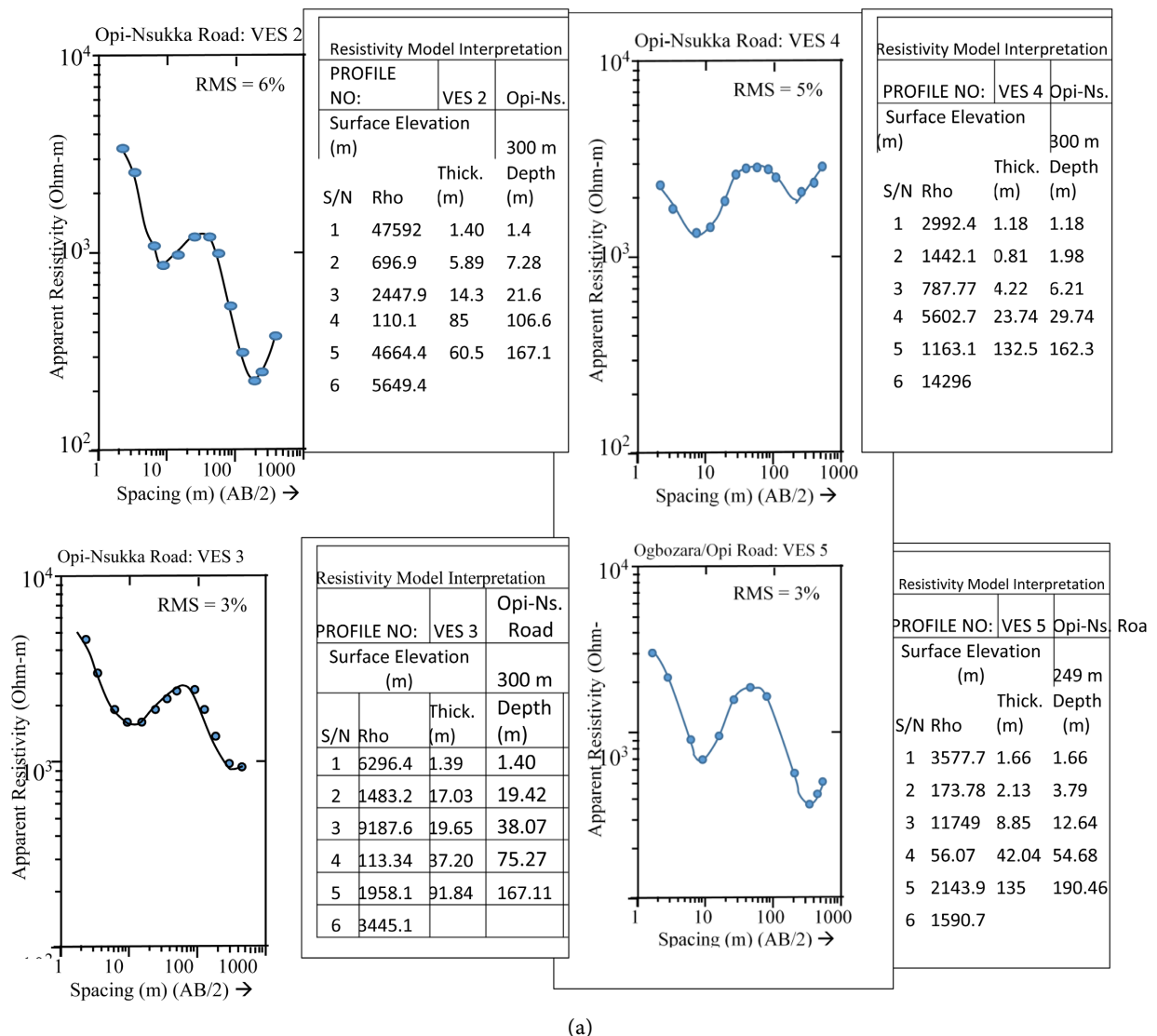
Subsequently, between a logging depth of 110 m and 125 m, the resistivity trend of the short and long normal resistivity logs increased significantly at the interface or boundary between the siltstone unit and the underlying silty sandstone layer, which is the fourth geo-electric zone and occurs between 125 and 170 m (**Figure 10**). In this fourth zone, the trend of the resistivity and SP curves increased and decreased, respectively, indicating that the upper to middle portions (125 to 145 m) of this zone non-water bearing. However, towards the basal section of this zone (145 m to 170 m), the resistivity and SP logs display downward decreasing and increasing trends, respectively (**Figure 10**). This suggests the presence of freshwater within the mid to lower parts of silty sandstone unit and a saturation that increases downward. The low resistivity recorded by VES 15 which is stationed close to this borehole supports a good water-bearing aquifer. This interval is viable for groundwater development.

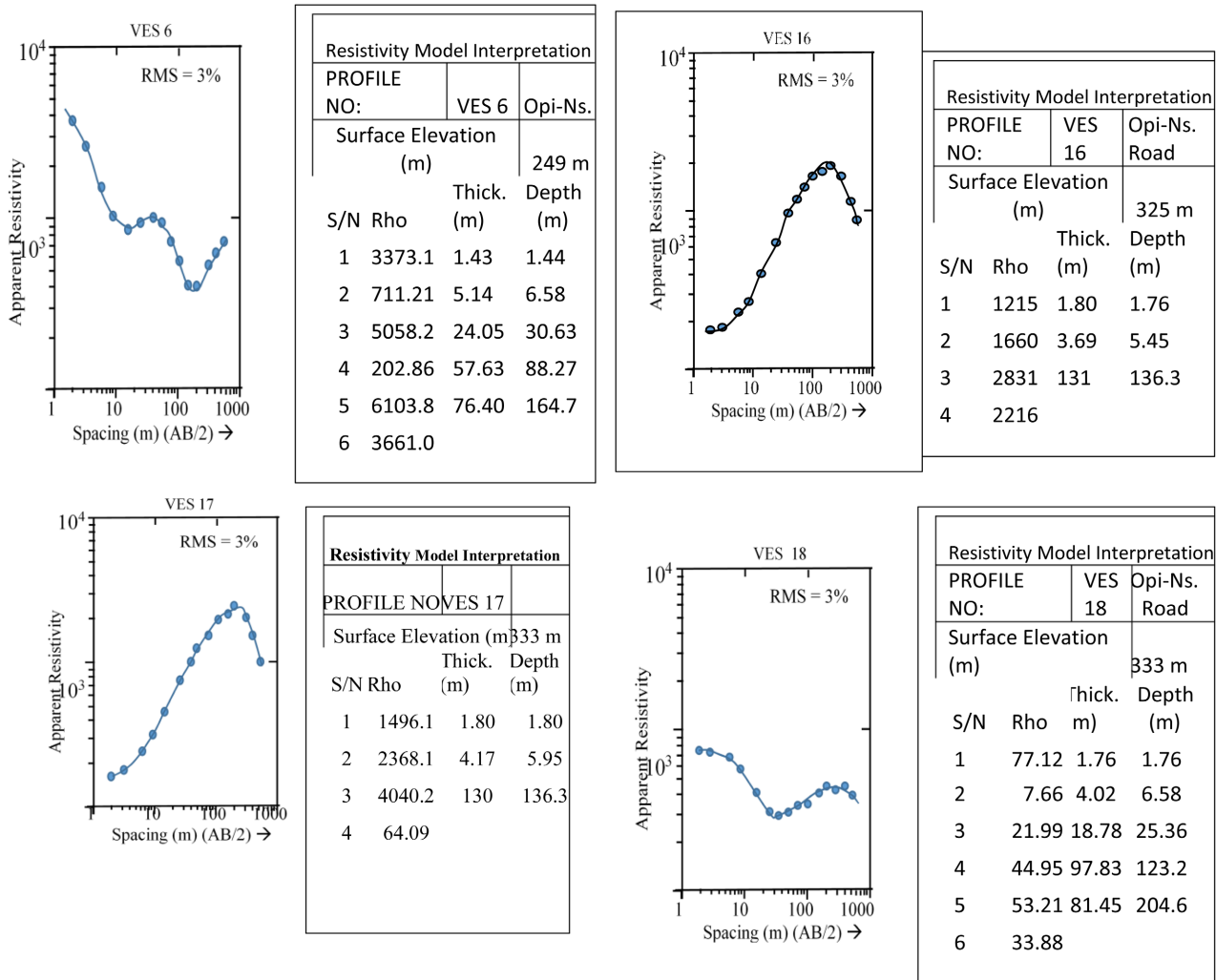
The fifth zone delineated by sub-surface geophysical logging is a thin bed of dark grey shale and clay that occurs between a logging depth of 170 and 175 m (**Figure 10**). The deflection of the resistivity and SP curves shows that the zone is wet. This could be attributed to the presence of clay materials within the shale

unit. Beyond the fifth zone downwards, the log-normal resistivity values increase slightly with a corresponding decrease in the trend of the SP curve, which indicates a decrease in saturation within the upper parts of the sixth layer, which comprises siltstone (175 to 190 m). Notwithstanding, between depth of 190 to 220 m, the deflection of the resistivity and SP curve supports the presence of a zone of saturation within the siltstone unit although the degree of saturation decreases downwards as the trend of the SP curve reduces downwards (Figure 10).

### 3.3. Interpretation of VES Data: 1-D Electro-Stratigraphic Models

The electro-stratigraphic model curves were obtained from the nineteen (19) VES data acquired in the study area to better understand the intricate physical properties of the underlying rocks beneath each sounding site and to ascertain key geophysical parameters characterizing each local subsurface structure. The underlying stratigraphies for all VES points located within each formation are displayed graphically in Figures 11-13 and the summary of the aquifer geo-electric





(b)

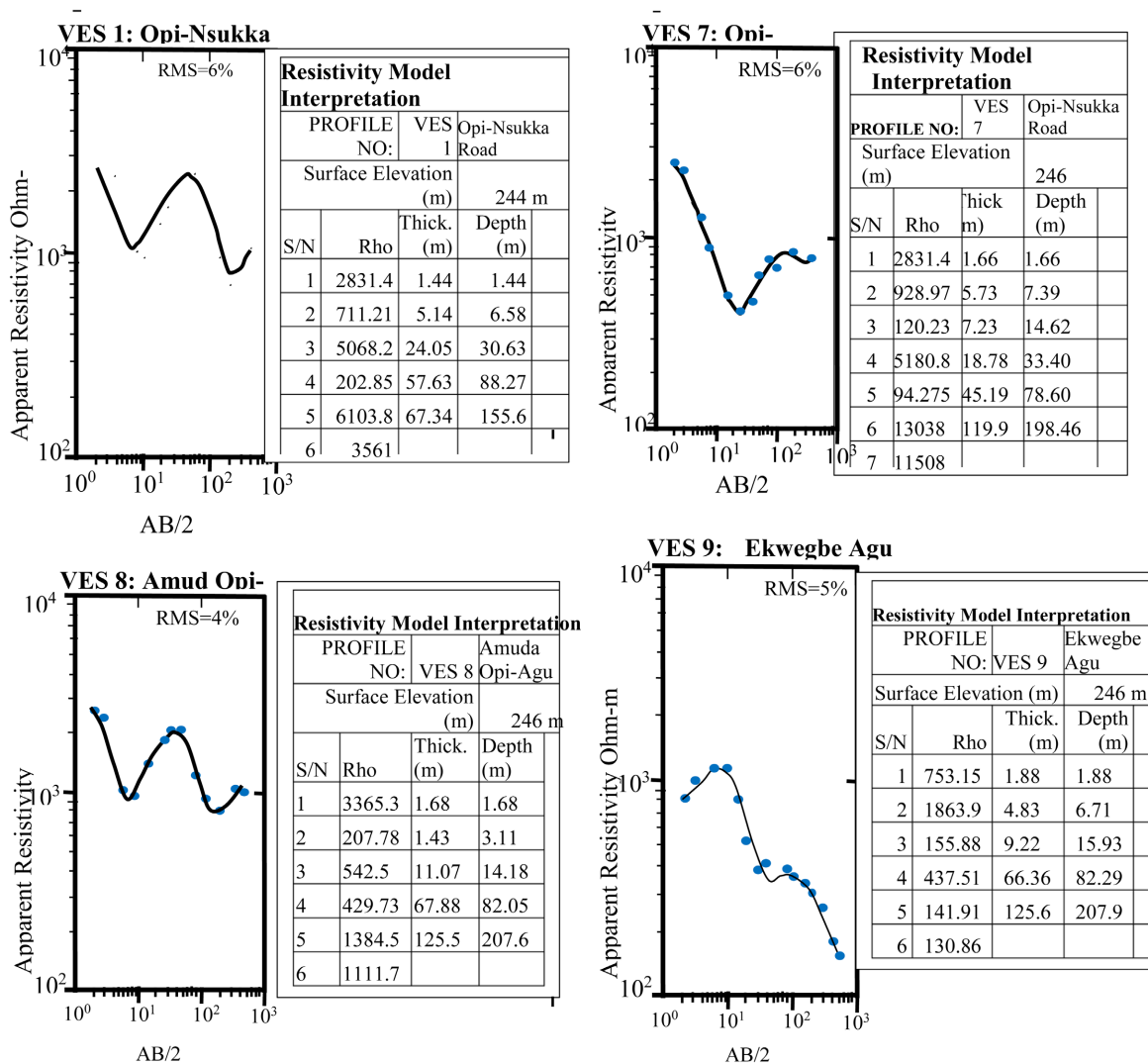
**Figure 11.** (a) Resistivity sounding curve showing geo-electric parameters beneath VES 2 - 5 drawn within Ajali Formation in the western and northwestern parts of the study. (b) Resistivity sounding curves showing geo-electric parameters beneath VES 6, 16, 17, 18 from sampling at Ajali Formation at the western and northwestern part of the study

parameters is presented in **Table 1**.

All the VES models obtained from resistivity sounding carried out within the Ajali Formation show a slightly close similarity in resistivity trend (an indication of a uniform sub-surface condition) but differ in their layer thicknesses, a function of the variation in thickness of geo-electric layers along the profiles (**Figure 11(a)**, **Figure 11(b)**). Six geo-electric layers were delineated across all the transects (VES 2, 3, 4, 5, 6 and 18) taken within the Ajali Formation except in VES 16 and 17 where four layers were observed. VES 3 - 5 indicate the HK curve type whereas VES 2, 6 and 18 show types AK, HKA and H curves respectively (**Table 1**). The six stratigraphic sequences observed beneath VES 2, 3, 4, 5, 6 and 18 are sand and clay heterolith, medium to coarse-grained sandstone, medium-grained sandstone, dark grey shale/siltstone and silty sandstone. The resistivity range of the topmost (thin) sand and clay horizon inferred from the stratigraphic curves

is between 2992.3 - 6286.4  $\Omega$ m. These very high resistivity values suggest that the sand and clay heterolith in VES 2, 3, 4, 5 and 6 is a dry zone (Figure 11(a), Figure 11(b)). Only VES 18 indicated a resistivity of 77.126  $\Omega$ m for this layer (Figure 11(a), Figure 11(b)). The low resistivity recorded could be attributed to the wet nature of the near-surface sand and clay unit, which is caused by its proximity to a nearby river. This low resistivity layer, which occurs within the medium-grained sandstone units and below the overlying unsaturated interval, represents the aquiferous zones in the VES models (Figure 11(a), Figure 11(b)). Thus, the range of depth to water for VES 2, 3, 4, 5, 6 and 18 within the Ajali Formation varies between 13 and 204 m with an aquifer thickness that ranges from 37 to 85 m (see Table 1).

The correlation of VES 5 with BH 1 shows remarkable agreement with the depth and thickness of the medium-grained sandstone aquifer. Data from BH 1 shown in Figure 9 indicates that the depth and thickness of the aquifer are 20 m and 35 m respectively compared to 12.64 m and 42.04 m observed in VES 5.



(a)

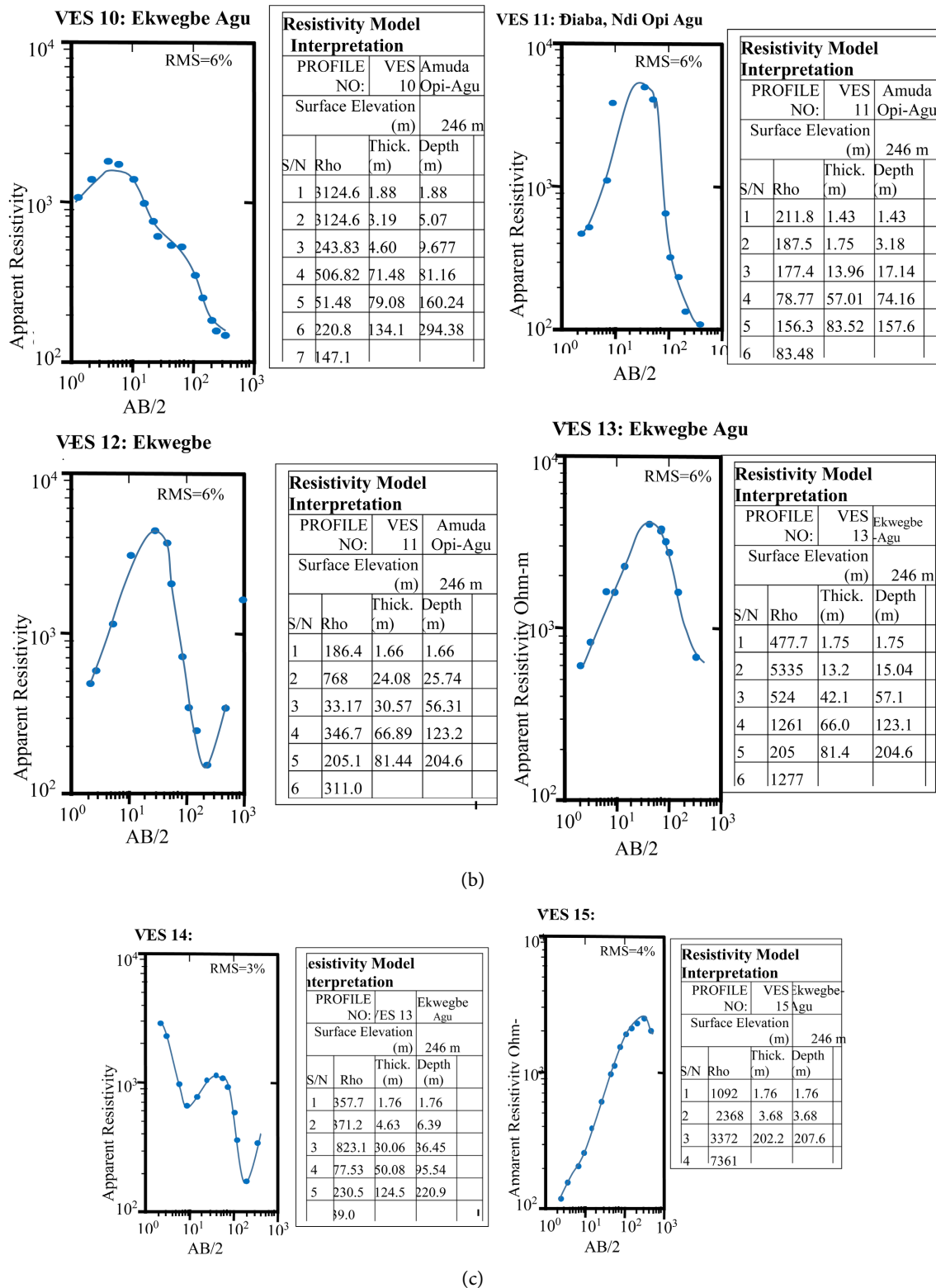


**Figure 12.** (a) Resistivity sounding curve showing geo-electric parameters beneath VES 1 and VES 7 - 9 drawn within Mamu Formation in the northeastern and southeastern parts of the study area; (b) Resistivity sounding curve showing geo-electric parameters beneath VES 10, 11, 12 & 13 drawn within Mamu Formation in the northeastern and southeastern parts of the study area; (c) Resistivity sounding curve showing geo-electric parameters beneath VES 14 - 15 drawn within Mamu Formation in the northeastern and southeastern parts of the study area.

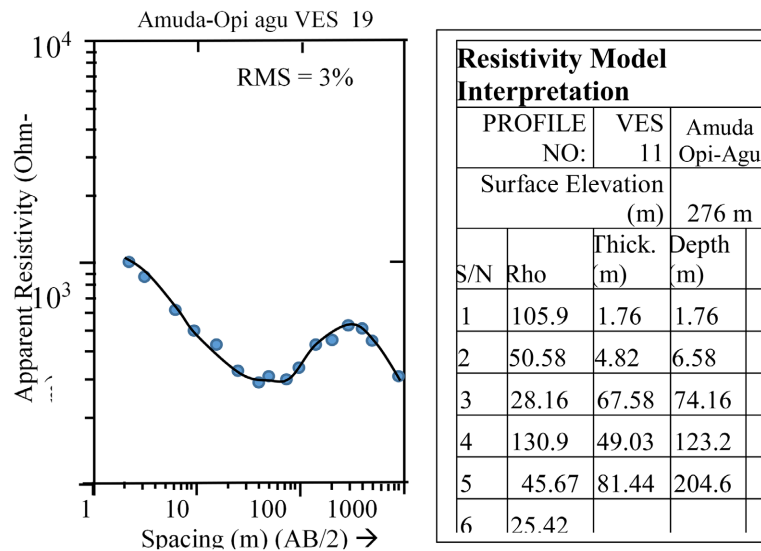


**Figure 13.** Resistivity sounding curve showing geo-electric parameters beneath VES 19 drawn within Enugu Formation in the southern fringes of the study area.

Locations of VES 16 and 17 (**Figure 11(b)**), run within the Ajali Formation are closely sited at the western part of the study area (**Figure 4**) and consist of four geo-electric layers unlike VES 2, 3, 4, 5, 6 and 18 which comprise six geo-electric layers. Both VES models show an AK curve type (see **Table 1**) and exactly similar resistivity trends with geo-electric depths and thicknesses that are identical (see **Figure 10(b)**). The three geological sequences established from the model curves of VES 16 and 17 are sand/clay heterolith, medium to coarse-grained sandstone and medium-grained sandstone that occupy the third and fourth geo-electric layers. The high resistivity (1715.5  $\Omega\text{m}$  and 1496.9  $\Omega\text{m}$ ) of the first geo-electric layer in both VES curves is similar to those observed in previous VES models taken within the Ajali Formation (see **Figure 10(b)**). By geological correlation, this unit represents the thin and topmost sand and clay heterolithic unit. In contrast with other curves described previously, the slightly lesser resistivities exhibited by this unit in VES 16 and 17 suggest a lower clay-to-sand ratio. The thickness of sand and clay heterolith in both electro-stratigraphic models is 1.76 m. The geo-electric layer underlying the heterolith occurs up to a depth of 5.45 and 5.95, respectively, in VES 16 and 17. This zone comprises dry sandstones of higher resistivities (1860.4 - 2368.1  $\Omega\text{m}$ ) that are medium to coarse grain in size. They are directly underlain by a zone of extremely high resistivity values that varies between 28,314 and 40,402  $\Omega\text{m}$  and coincides with the third geo-electric layer in VES 2, 3, 5 and 6, and the fourth geo-electric layer in VES 4 representing the very dry unsaturated (vadose) zone within the medium-grained sandstone (see **Figure 11(a)** & **Figure 11(b)**). In contrast to other VES results obtained within the Ajali Formation, the depth to water beneath VES 16 and 17 (136 m); (**Table 1**) is exceptionally high and is probably due to the large thickness of the overlying vadose zone (130.88 m and 130.39 m) caused by the high surface elevation (325 m and 333 m) at the VES stations (**Figure 10(b)**).

VES 1, VES 7, and VES 8 - 15 were sampled within the Mamu Formation (**Figures 12(a)-(c)**), while VES 1 and 15, VES 11 and 13, and VES 9 - 10 show the AK, K and KHQ curve types, respectively, VES 7, 8, 12, and 14 indicate types QK, HK, KA and HKA curves (**Table 1**). The wide variation in curve types could be attributed to the variation in geo-electric characteristics of the sub-surface electro-stratigraphic units at these VES points, which was caused by the highly heterogeneous nature of the Mamu Formation in the study area. Excluding VES 7, 10 and 15, all the VES models drawn within this formation display six geo-electric layers. VES 7 and 10 show seven geo-electric layers (**Table 1**). Only VES 15, which was sited close to BH 2, shows four geo-electric layers (see Figs 12a-c). Of all the VES models having six geo-electric layers, VES 9, 12 and 13 are closely located and show a similar trend in resistivity values (**Figure 12(a)** & **Figure 12(b)**). The six geo-electric layers that underlie VES 1 and VES 8 - 14 correspond to lateritic overburden, dark grey shale/siltstone, silty sandstone, siltstone, dark grey shale/clay and siltstone. However, in VES 11, the thin dark grey shale/clay sequence was not observed. In this case, a layer of silty sandstone was present beneath the siltstone unit that occupies the fourth geo-electric layer in this model. In the VES models, the resistivity range of the lateritic overburden varies between 186.38 and 3385.3  $\Omega\text{m}$  (see **Figures 12(a)-(c)**). While the VES 11 - 13, whose resistivities are 211.84  $\Omega\text{m}$ , 186.38  $\Omega\text{m}$  and 477.75  $\Omega\text{m}$ , respectively, the thin-dry overburden layer is characterized by high resistivity values. A closer observation at BH 2 clearly shows that the range of logging depth is between 30 and 260 m (see **Figure 10**). This implies that most of the sub-surface drilling was done within the zone of silty sandstone, which is characterized by extremely high resistivity values. Although electrical sounding could not readily decipher the variation in resistivity within this layer, data obtained from BH 2 showed a fluctuation in the degree of saturation within this zone caused by the supposedly heterogeneous nature of this unit. This is evident by the deflection of the long normal resistivity log, which probes the deeper part of the silty sandstone unit (see **Figure 10**). This interval may be a zone of infiltration overlying the low resistivity (7351.9  $\Omega\text{m}$ ) aquifer that occupies the fourth geo-electric unit (see **Figure 12(c)**). The drastic drop in the resistivity of the fourth geo-electric suggests that the siltstone sequence underlying the silty sandstone unit represents the aquiferous unit beneath VES 15. By fair approximation, the depth of this aquifer as recorded in VES 15 (208 m) and BH 2 (190 m) shows reasonable agreement. The depth to water (208 m) beneath VES 15 is the greatest when compared to other sounding models (see **Table 1**). This could be attributed to the thickness of the infiltration zone (202.23 m) as well as the high elevation (346 m) at this VES point (see **Figure 12(c)**).

The electro-stratigraphic parameters of different geo-electric layers beneath VES 19 drawn at the southern fringes of the study area within the Enugu Formation are shown in **Figure 13**. Six geo-electric layers were identified beneath the type H curve of the VES model (see **Table 1**). The assigned geological meanings of the electro-stratigraphic layers from top to bottom are lateritic

overburden, dry grey shale, thick and wet grey shale, dry grey shale, and fractured shale. The fifth and sixth geo-electric layers comprise a single geological sequence.

The thin and dry lateritic overburden has a resistivity of 105.88  $\Omega\text{m}$ . Below this layer, the resistivity of the second geo-electric layer reduces to 50.582  $\Omega\text{m}$  up to a depth of about 6.58 m. The low resistivity value encountered here is an indication of the presence of grey shales that are wet but not saturated. Similarly, the occurrence of low resistivity (28.158  $\Omega\text{m}$ ) shales as indicated by the third geo-electric layer implies the presence of a thick unit of light grey shales that are wet (**Figure 13**). The higher degree of wetness within this layer could be attributed to the presence of numerous fractures within the thick shale unit. Beneath this unit is a layer of higher resistivity (130.86  $\Omega\text{m}$ ) that consists of dry grey shales, which is the fourth geo-electric layer. Further downward, between a depth of 123.20 m and 204.64 m, a shale unit of very low resistivity value is observed. This unit comprises the fifth geo-electric layer and appears to extend downward as the resistivity reduces up to the sixth geo-electric layer. This unit is interpreted as highly fractured shales that contain enormous water resources that are suitable for borehole drilling and development (see **Figure 13**). The decrease in resistivity downward up to the sixth geo-electric layer suggests a downward increase in saturation and is desirable for borehole placement. This aquifer has a determined depth and thickness of about 123.2 m and 81 m respectively.

### 3.4. A 2D Modeling and Geologic Correlation of Sounding Curves

The VES curves were correlated based on the range of resistivity values for the inferred unit lithologies. Resistivity information was concentrated along these unequal-spaced stations to produce a fairly systematic data array. Afterwards, a geologic interpolation was made for each sounding curve, and the interpretation was projected in a step-wise pattern to adjoining curves. This is to provide a better understanding of the continuity of the aquiferous system.

Profile 1, which covers the Ajali and Mamu formations, traverses the centre of the study area in an NW-SE direction (see **Figure 4**) and connects three VES stations (VES 4, VES 11 and VES 15) and one borehole point (BH 2), with a centre that passes through the southeastern part of Opi. **Figure 14(a)** shows the lithological correlation of the VES models and borehole data, and the resulting two-dimensional sub-surface geological model beneath this profile is shown in **Figure 14(b)**. The aquifer material beneath VES 4 (Ajali Formation) is the medium-grained sandstone unit while the silty sandstone unit is the water-bearing layer beneath VES 11 (Mamu Formation). In BH 2 and VES 15, the basal unit of siltstone within the Mamu Formation constitutes the target aquifer (**Figure 14(b)**). Unlike VES 4, the aquifer layer underlying VES 11, BH 2 and VES 15 in Mamu Formation, shows evidence of lateral continuity in the southeastern direction. On the other hand, the medium-grained sandstone aquifer beneath VES 4 is laterally continuous with a thickness that increases in the northwestern

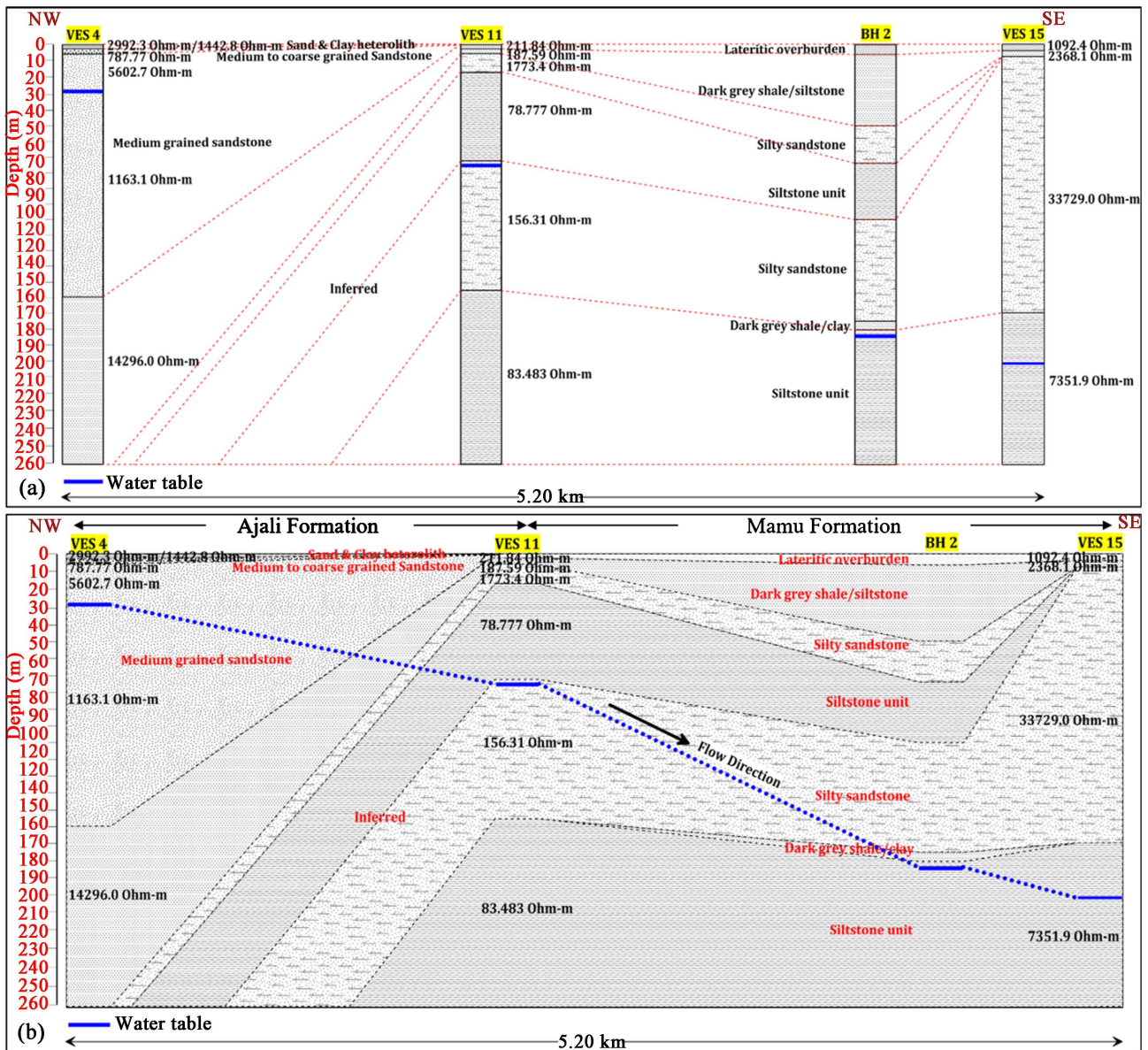


**Figure 14.** (a) Correlation of VES and borehole data along Profile 1 (b) 2D geological model along Profile 1 showing the direction of groundwater flow.

direction. However, it pinches out towards the southeastern part as one approaches VES 11, indicating a gradual transition from the Ajali Formation at the northwest to the Mamu Formation in the southeast (Figure 14(b)). Although the thickness of the silty sandstone aquifer underlying VES 11 increases towards the southeast, same cannot be said of the siltstone aquifer (in BH 2 and VES 15) whose thickness decreases slightly in the same direction. The 2D model indicates a NW-SE groundwater flow direction with the water table being shallowest at the northwestern side of the profile, which is underlain by the Ajali Formation. This suggests that the groundwater flow direction is controlled by elevation as water flows from the highly elevated Ajali Formation at the NW to the less elevated Mamu Formation in the SE (Figure 14(a) & Figure 14(b)).

Profile 2 connects four VES stations (VES 5, VES 7-8 and VES 13) at the southern part of the study area and traverses a horizontal length of about 5 km (see Figure 4; Figure 15(a)). It assumes a roughly WSW-ENE direction and cuts across the Ajali and Mamu formations. Most of this profile is underlain by Mamu Formation, especially on the eastern side where it intersects with Profile 1 at the midpoint between VES 7 and 8. The profile traverses only a section of the Ajali Formation at the western part of VES 5 and VES 7 (see Figure 4). The western section of this profile shows closely similar geometry and bed properties to that of Profile 1. The medium-grained sandstone facies here also serve as the aquiferous unit in VES 5 with a shallow water table (<15 m) (Figure 15(b)). It thickens and thins out in the southwest and southeast directions respectively. This implies that the aquifer layer is only likely to be continuous in the south-western away from the Mamu Formation. Conversely, the silty sandstone aquifer underlying VES 7 and 8 occurs at slightly deeper intervals (14 and 33 m respectively) within the Mamu Formation and is laterally continuous. However, it thickens slightly between VES 7 and 8 but appears to gradually thin out beyond

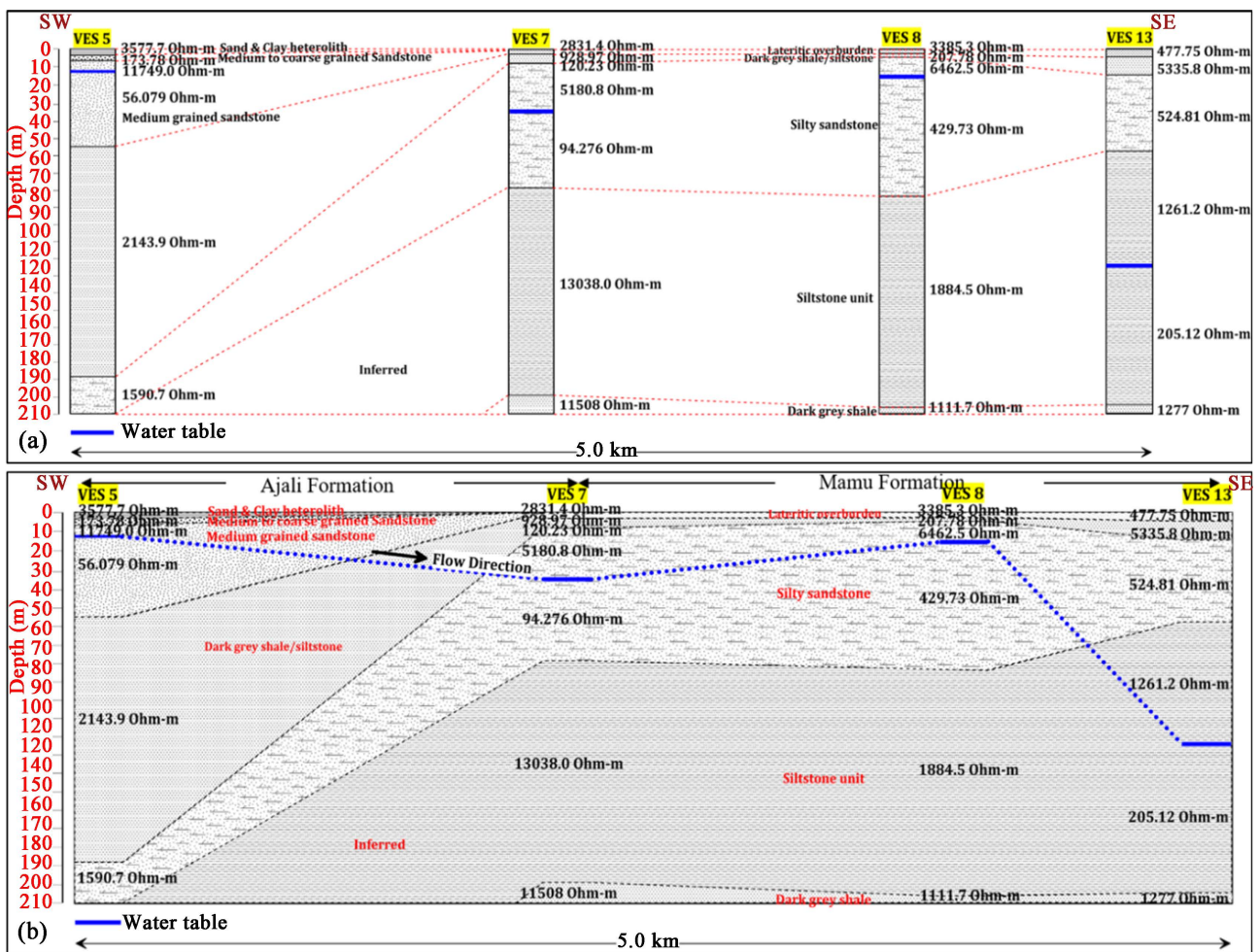


Figure 15. (a) Correlation of VES data along Profile 2 (b) 2D geological model along Profile 2 showing the direction of groundwater flow.

VES 13 (Figure 15(b)). The siltstone unit, which represents the aquiferous unit beneath VES 13, is laterally continuous with a thickness that increases in the southeastern direction away from the boundary between the Ajali and Mamu Formations. The water table here is deeply located (123 m) and suggests an SW-SE direction of groundwater flow beneath the profile (Figure 15(b)) from the Ajali Formation to the Mamu Formation. The direction of groundwater flow is controlled by elevation.

The 2D geological model of the sub-surface along this profile indicates shallow water levels at the southwestern part and deeper water levels at the eastern side.

Profile 3 is drawn at the centre of the study area in a direction that is orthogonal and parallel, respectively, to Profiles 1 and 2. It covers a horizontal distance of about 6.5 km in a roughly west-to-east direction (see Figure 4) while connecting VES 3, 2, 11 and 9 - 10 in the same direction (Figure 16(a)). While VES 2 and 3 are domiciled within the Ajali Formation, VES 9 - 11 are stationed within the Mamu Formation in a straight line, east of VES 2 and 3. The western part of this profile appears to show a similar geometry to the models in the profiles

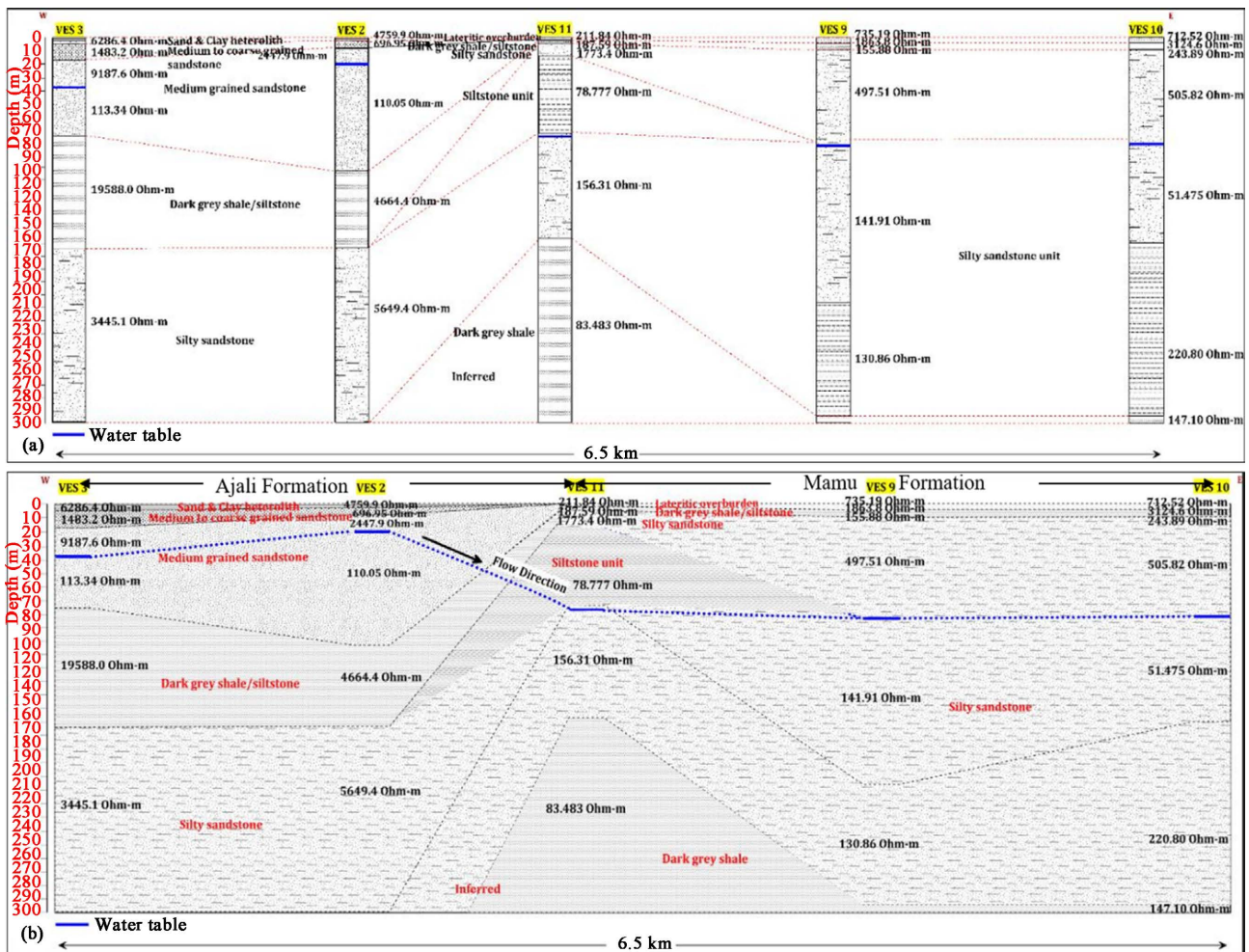


Figure 16. (a) Correlation of VES data along Profile 3 (b) 2D geological model along Profile 3 showing the direction of groundwater flow.

that have been previously described. The only exception is that the medium-grained sandstone unit that serves as a groundwater reservoir beneath VES 2 and 3 appears to gradually thin out in the western direction even though it is thickly bedded and laterally extensive (**Figure 16(b)**). Similarly, the water table (22 and 28 m) beneath VES 2 and 3 located within the Ajali Formation is shallower compared to those at the VES stations positioned within Mamu Formation where the water table indicates very closely related values (74 - 82 m). This is attributed to the difference in elevation at the ground surface in both formations. The silty sandstone aquifer that underlies VES 9-11 at the eastern part of the profile is also thick and laterally continuous. However, the thickness of the aquifer material increases slightly from VES 11 to VES 9 after which it slightly decreases up to the eastern edge of the model (**Figure 16(b)**). This silty sandstone aquifer, which covers over 90% of the sub-surface within the Mamu Formation, is overlain and underlain by dark grey shales. This suggests that the silty sandstone layer is a confined aquifer system. The correlation of the water level inferred from the VES models along this profile shows that groundwater flows in a west-to-east direction under gravity (Figs 16a-b).

Profile 4 commences at VES 6 where it stretches obliquely from the southwestern part of the study area and terminates at the northeastern part in VES 14 (see **Figure 4**). It links four equal-spaced VES stations (VES 6, VES 2, VES 12 and VES 14) that cuts across Idi, Opi and Ogbozara localities. The profile traverse runs through the Ajali and Mamu formations and covers a surface distance of 6.9 km with Opi town at its midpoint (**Figure 17(a) & Figure 17(b)**). It shows a similar sub-surface architecture with profiles 1 and 3. VES 2 and 6 are underlain by the sediments of the Ajali Formation while VES 12 and 14 are underlain by the more heterogenous sediments of the Mamu Formation (**Figure 17(b)**). The medium-grained sandstone unit is the recognized aquifer beneath VES 2 and 6 where it is thickly bedded and lateral continuous. The depth to water within the 107 m thick sediments is quite shallow and ranges between 22 and 33 m beneath the VES stations. On the other hand, the silty-sandstone interval underlying the dark grey shale/siltstone layer represents the aquiferous layer beneath VES 12 and 14 (**Figure 17(b)**). Although the water table appears relatively shallow (26 - 36 m) below these VES stations, the thickness of the aquifer increases from VES 2 to VES 12 in the northeast direction and remains uniform beyond VES 12. The overlying and underlying dark grey shales create a confining aquiferous system beneath these VES locations. The direction of groundwater flow as determined in Profile 4 is SW to NE with elevation playing a huge role in influencing the groundwater flow direction.

From the four profiles, the regional flow direction of groundwater in the study area is west to east.

### **3.5. Evaluation of Aquifer Hydraulic Properties**

#### **Distribution of Aquifer Resistivity**

The resistivity of the main aquifer units underlying the study area is generally

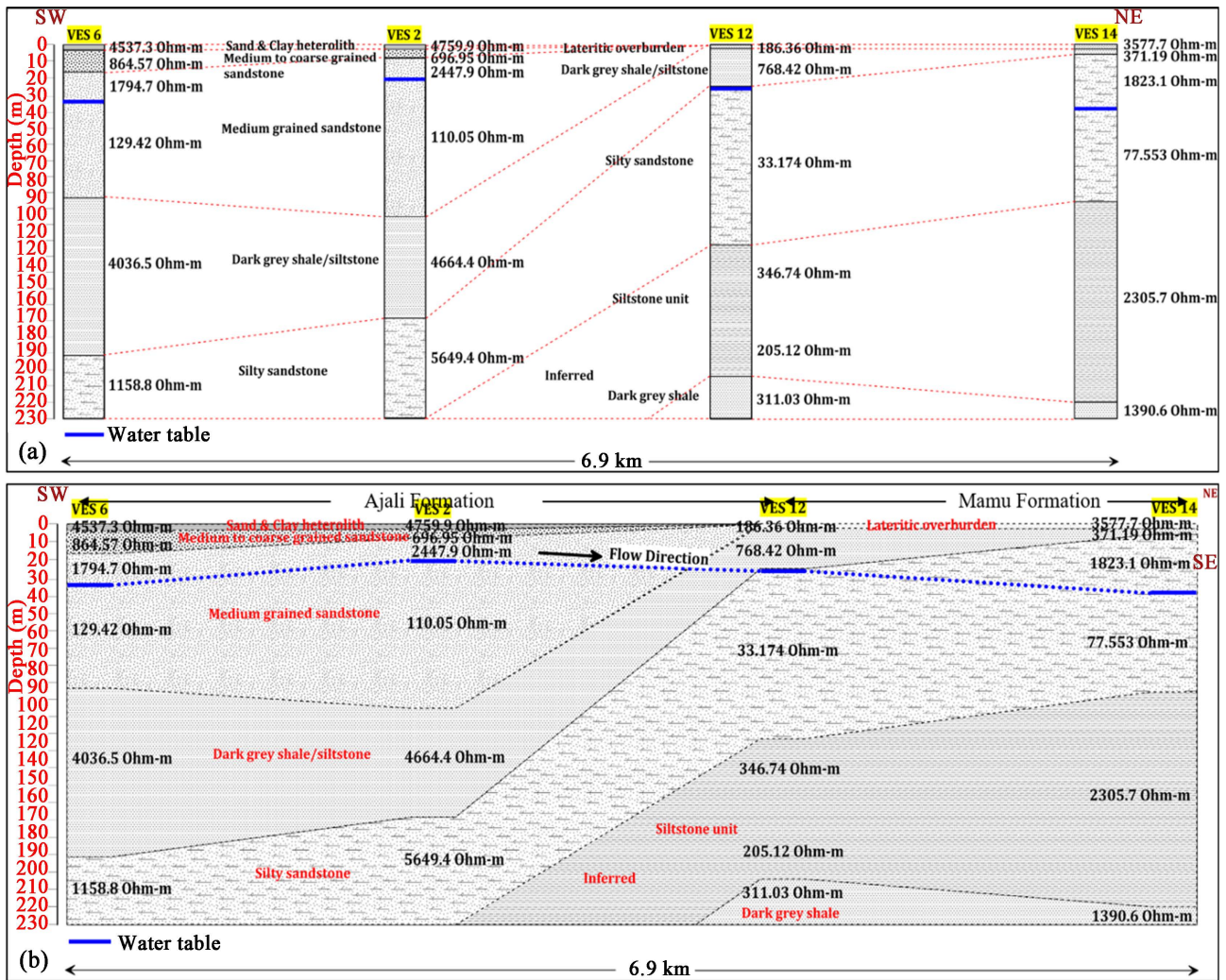
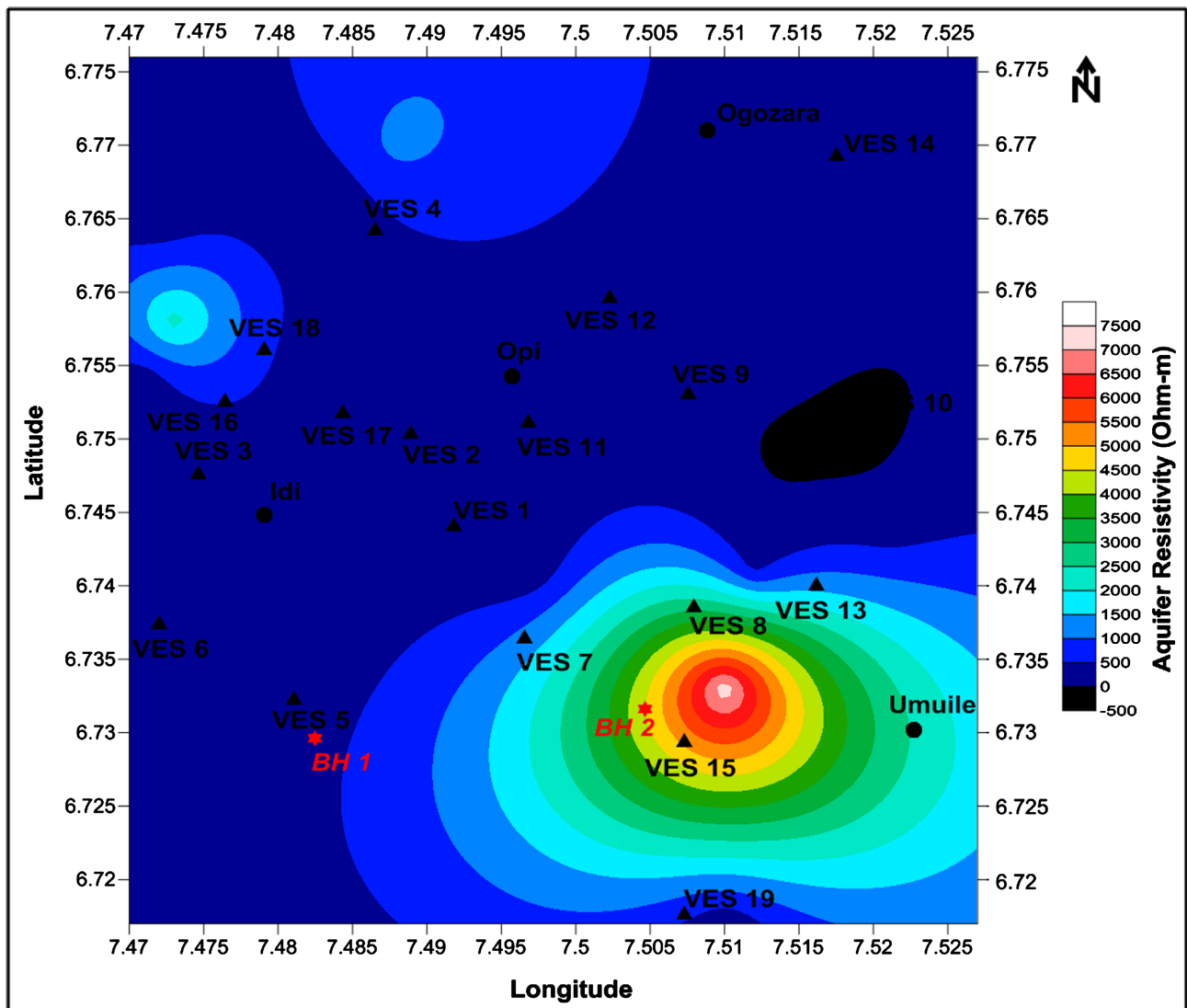


Figure 17. (a) Correlation of VES data along Profile 4 (b) 2D geological model along Profile 4 showing the direction of ground-water flow.

low with values that vary between 1 and 500  $\Omega$ m, especially at the western, central and northeastern parts of the study area (Figure 18). These areas comprise the medium grain sandstone aquifer within the Ajali Formation as well as the silty sandstone and siltstone aquifers that occur in the Mamu Formation (see Figure 4). Of these areas, a small section of the northwestern fringes of the study area, west of VES 16 and 18 reveal a slightly higher aquifer resistivity within the Ajali Formation in the range of 100 to 2000  $\Omega$ m. VES 16 shows an aquifer resistivity of 2216  $\Omega$ m. Depths to water at VES 16 and 18 ranged between 136 and 205 m. Similarly, a slight increase in the resistivity (500 - 1000  $\Omega$ m) of the aquifers located within the Ajali and Mamu formation at the northwestern/north-central axis, was observed. The highest aquifer resistivities (2000 - 8000  $\Omega$ m) occurred within the Enugu Formation in the southeastern part of the study area (Figure 18) where depths to the water table were observed to be higher. Most areas with shallow water depths were characterized by low aquifer resistivities and vice-versa.



**Figure 18.** Contour map showing high aquifer resistivities predominantly in the southeastern region and partly in the northwestern region of the study area.

### 3.6. Distribution of Aquifer Depth

The deepest aquifers within the study area occur in the northwestern and southeastern parts, which are underlain by sediments of the Ajali and Enugu Formations, respectively (Figure 19). Aquifer depths appear to increase progressively in the northwestern and southeastern directions, which correlate reasonably well with zones of higher aquifer resistivity (see Figure 19). Also, the direction of increasing aquifer depths coincides with the direction of decreasing elevation, which supports a west to east direction of regional groundwater flow, as shown in the 2D sub-surface geological models (see Figures 14-17). This suggests that the study area is probably close to a watershed with two drainage areas located at the northwest and southeast of a cuesta that possibly trends in a roughly NNE-SSW direction (See Figure 20) Opi town appears to be close to the foot of the escarpment, southeast of the cuesta, with Umuile lying on the gentle area

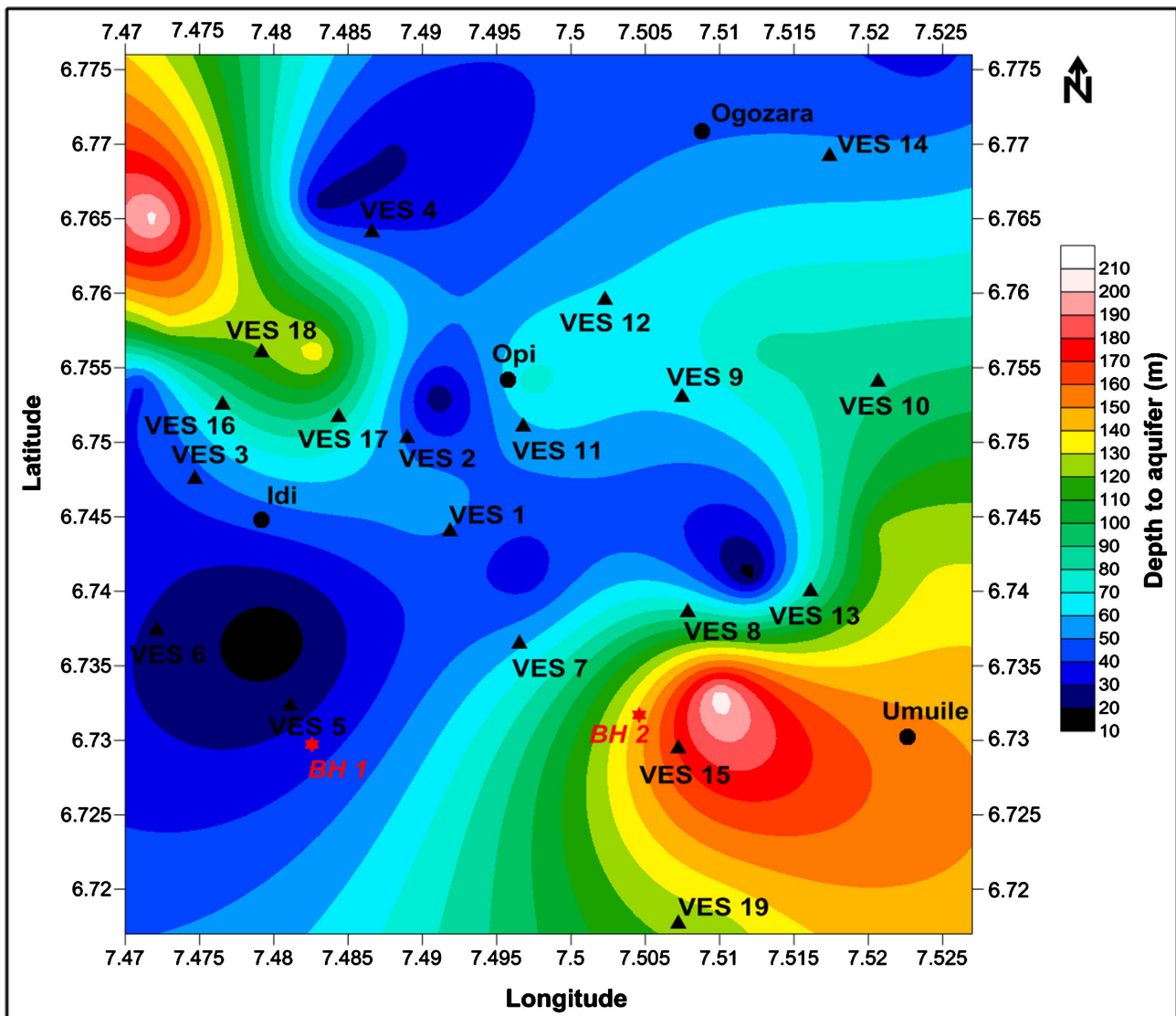


**Figure 19.** Contour map showing a progressive increase in aquifer depth towards the northwestern and southeastern directions which reflects the regional direction of groundwater flow and depicts a watershed.

(plateau) (see [Figure 5](#)). The cuesta is the well known as the Udi-Nsukka cuesta.

### 3.7. Distribution of Aquifer Thickness

Aquifer thickness increases from the southwestern to the northeastern part of the study area ([Figure 21](#)). The aquifer units in the northwestern and southwestern axis vary between 30 and 65 m. Aquifer thickness at the southeastern section is moderate and ranges from 65 to 90 m. The thickness units of aquifer materials occur at the north-central and north-eastern part of the study area with a thickness that varies between 95 and 140 m ([Figure 21](#)). Most parts of the Ajali Formation especially at the western and southwestern regions have the lowest aquifer thicknesses. This is due to the generally lesser thickness of the Ajali Formation (compared to the Mamu Formation) at these locations, which is indicated in the 2D geological models (see [Figures 14-17](#)).

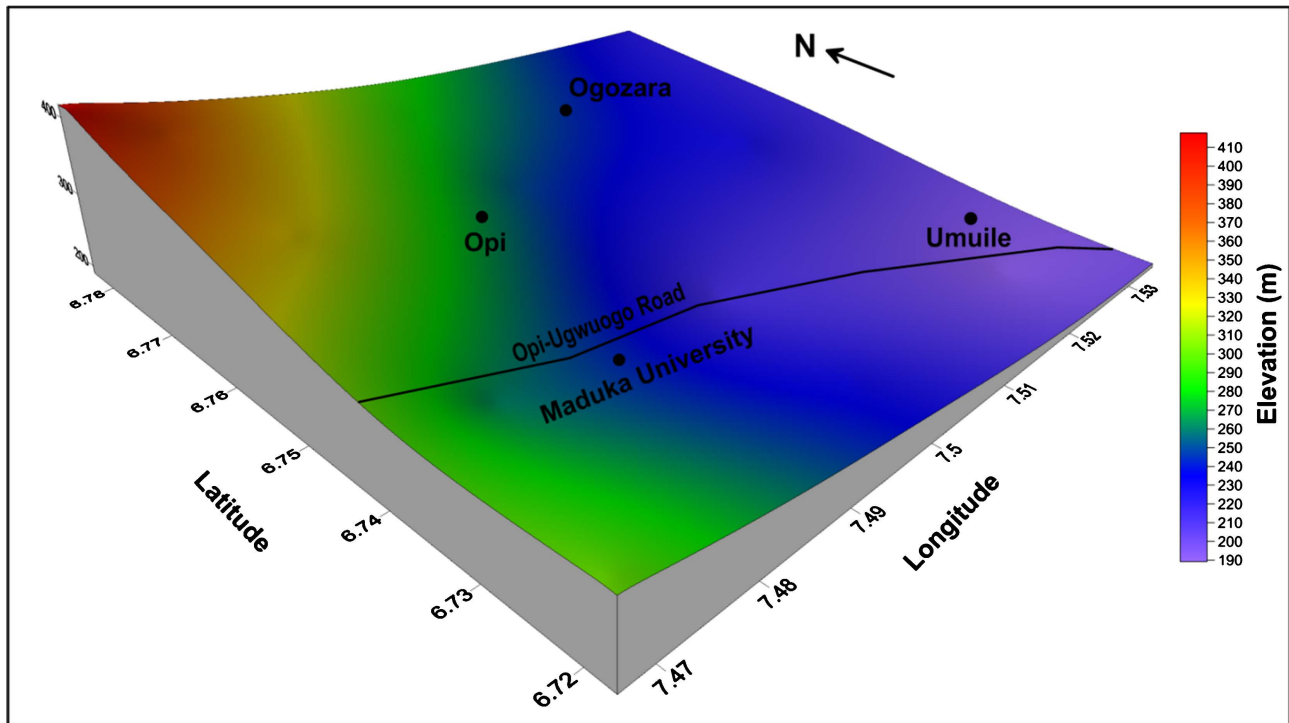


**Figure 20.** Digital Elevation Model of the study area showing higher relief at the western part.

#### 4. Conclusions

Geological and borehole data as well as information from ground geophysical measurements have been successfully integrated in investigating the sub-surface geological formations within Ekwegbe-Agu and environs, Enugu state Nigeria, for groundwater resources.

The geological mapping of the study area revealed three (3) prominent geologic Formations; Enugu Formation, Mamu Formation and Ajali Formation respectively.

The dominant curve type obtained from the different formations is the AK curve type followed by the HK curve type respectively while an average of six geo-electric layers were delineated across all transects taken with resistivity values ranging from 25.42 - 105.85  $\Omega\text{m}$  in the Enugu Shale, 186.38 - 3383.3  $\Omega\text{m}$  in the Mamu Formation and 2992.3 - 6286.4  $\Omega\text{m}$  respectively.

The 2D model indicates a NW-SE groundwater flow direction which suggests that the groundwater flow direction is controlled by elevation as water flows from the highly elevated Ajali Formation at the NW to the less elevated Mamu Formation in the SE.

The resistivity of the main aquifer units underlying the study area is generally low and the resistivity of the aquifer seems to be directly proportional to the aquifer depth in the study area. Also, the aquifer thickness model shows that a portion of the Ajali Formation within the north-western areas and west of Ogozara possesses a thick aquiferous interval which closely agrees with the 2D stratigraphic models described.

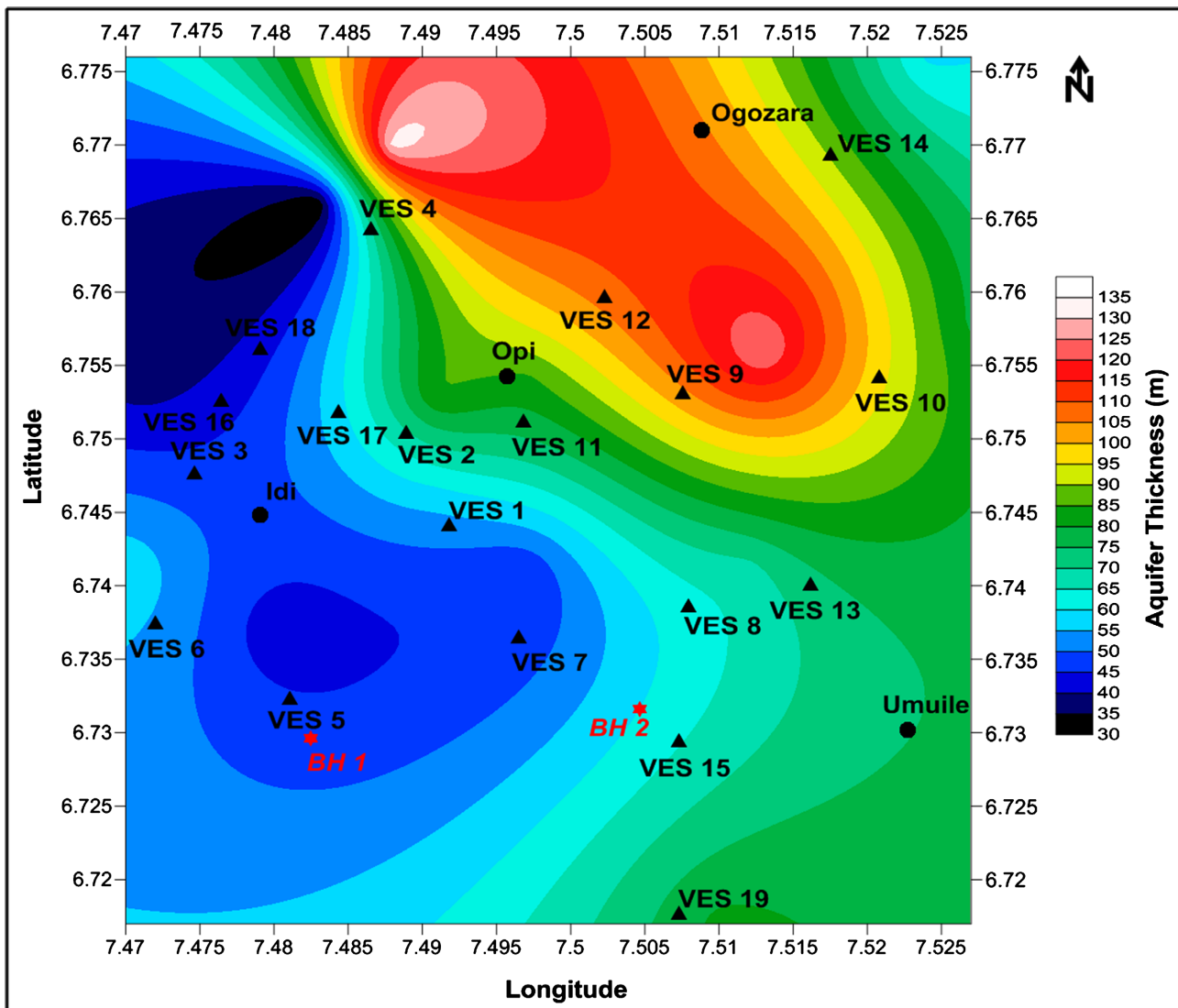


**Figure 21.** Contour map showing the increase in aquifer thickness from the southwestern part to the northeastern part of the study area.

Therefore the western and northwestern part of the study area which is underlain mainly by the Ajali Formation showed the highest groundwater potential in the study area and should be targeted for high-yield borehole placement in the study area. Depths exceeding 130 m are recommended for boreholes sited within that axis of the study area.

### Acknowledgements

The authors acknowledge, with thanks, the efforts of the crew members of Felgra Links Nigeria Limited during the surface geophysical data acquisition and for providing the borehole logging data used for this study.

### Conflicts of Interest

The authors declare no conflicts of interest regarding the publication of this paper.

## References

- [1] MacDonald, A., Davies, J., Calow, R. and Chilton, J. (2005) *Developing Groundwater: A Guide for Rural Water Supply*. ITDG Publishing, London, 358. <https://doi.org/10.3362/9781780441290.000>
- [2] Delleur, J.W. (2006) *The Handbook of Groundwater Engineering*. CRC Press, Boca Raton. <https://doi.org/10.1201/9781420006001>
- [3] Ezeh, C.C. (2012) Hydrogeophysical Studies for the Delineation of Potential Groundwater Zones in Enugu State, Nigeria. *International Research Journal of Geology and Mining*, **2**, 103-112.
- [4] Hassan, L., Abdellatif, M. and Moumtaz, R. (2017) Modelling of Transient Two-Dimensional Flow in Saturated-Unsaturated Porous Media. *European Science Journal*, **13**, 195-213. <https://doi.org/10.19044/esj.2017.v13n12p195>
- [5] Zohdy, A.A.R., Eaton, G.P. and Mabey, D.R. (1974) *Application of Geophysical Methods to Groundwater Investigation: Techniques of Water-Resources Investigation of the United States Geological Survey*. U.S. Geological Survey, Reston.
- [6] Ezeh, C.C., Ugwu, G.Z., Okonkwo, A. and Okamkpa, J. (2013) Using the Relationships between Geoelectrical and Hydrogeological Parameters to Assess Aquifer Productivity in Udi LGA, Enugu State, Nigeria. *International Research Journal of Geology and Mining*, **3**, 9-18.
- [7] Oladele, S. and Odubote, O. (2017) Aquifer Mapping and Characterization in the Complex Transition Zone of Ijebu Ode, Southwestern Nigeria. *Forum Geografic*, **16**, 49-58. <https://doi.org/10.5775/fg.2017.112.i>
- [8] Amadi, A.N., Nwawulu, C.D., Unuevho, C.I., Okoye, N.O., Okunlola, I.A., Egharevba, N.A., Ako, T.A. and Alkali, Y.B (2011) Evaluation of the Groundwater Potential in Pompo Village, Gidan Kwano, Minna Using Vertical Electrical Resistivity Sounding. *Current Journal of Applied Science and Technology*, **1**, 53-66. <https://doi.org/10.9734/BJAST/2011/192>
- [9] Abiola, O., Enikanselu, P.A. and Oladapo, M.I (2009) Groundwater Potential and Aquifer Protective Capacity of Overburden Units in Adoekiti, Southwestern Nigeria. *International Journal of Physical Sciences*, **4**, 120-132.
- [10] Oseji, J.O. and Ujuanbi, O. (2009) Hydrogeophysical Investigation of Groundwater Potential in Emu Kingdom, Ndokwa Land of Delta State, Nigeria. *International Journal of Physical Sciences*, **4**, 275-284.
- [11] Amah, J.I. (2006) *Mathematical Modelling of Groundwater Flow System of a Water Table Aquifer in Nsukka Area, Southeastern Nigeria*. University of Nigeria Research Publication, Nsukka, 56-62.
- [12] Onwe, M.R., Abraham, E.M., Ambrose, N.T. and Osike, O.K. (2022) An Evaluation of the Hydrogeology Potential of Nsukka, Southern Nigeria, Using Geographic Information System. *Applied Water Science*, **12**, Article No. 54. <https://doi.org/10.1007/s13201-022-01579-6>
- [13] Uzoije, A.P., Onunkwo, A.A., Ibeneme, S.I. and Obioha, E.Y (2014) Hydrogeology of Nsukka Southeast—A Preliminary Approach to Water Resources Development. *American Journal of Engineering Research*, **3**, 150-162.
- [14] Nwankwor, G.I., Egboka, B.C.E. and Orajaka, I.P. (1988) Groundwater Occurrence and Flow Patterns in the Enugu Coal Mines Area, Anambra State, Nigeria. *Hydrological Sciences Journal*, **33**, 465-482. <https://doi.org/10.1080/02626668809491275>
- [15] Ugbor, C.C. and Nnadi, A.L. (2020) Integration of Geophysical Techniques for Groundwater Investigation around Obollo-Afor, Southeastern Nigeria. *Proceedings*

of the 56th Annual International Conference & Exhibitions of the Nigerian Mining and Geosciences Society (NMGSS), Ibadan, 22-27 March 2020, 462-468.

- [16] Nwachukwu, C.C., Ugbor, C.C. and Ogboke, J.O. (2022) Electrical Resistivity Sounding for Groundwater Investigation around Enugu Metropolis and the Environs, Southeast Nigeria. *International Journal of Geosciences*, **13**, 54-70.  
<https://doi.org/10.4236/ijg.2022.131004>
- [17] Chiaghanam, O.I., Chiadikobi, K.C., Ikegwuonu, O.N., Omoboriowo, A.O., Onyemesili, O.C. and Acra, E.J. (2013) Palynofacies and Kerogen Analysis of Cretaceous (Early Campanian-Maastrichtian) Enugu Shale and Mamu Formations in Anambra Basin, Southeastern Nigeria. *International Journal of Scientific and Technology Research*, **2**, 225-229.
- [18] Wright, J.B., Hastings, D.A., Jones, W.B. and Williams, H.R (1985) *Geology and Mineral Resources of West Africa*. George Allen and Unwin, London, 190.
- [19] Nwajide, C.S. (2005) Anambra Basin of Nigeria: Synoptic Basin Analysis as a Basis for Evaluation of Its Hydrocarbon Prospectivity. In: Okogbue, C.O., Ed., *Hydrocarbon Potentials of the Anambra Basin*, Great AP Express Publishers Ltd., Nsukka, 2-46.
- [20] Nwajide, C.S. and Reijers, T.J.A. (1996) Geology of the Southern Anambra Basin. In: Reijers, T.J.A., Ed., *Selected Chapters on Geology*, SPDC, Warri, 133-148.
- [21] Tijani, M.N., Nton, M.E. and Kitagawa, R. (2010) Textural and Geochemical Characteristics of the Ajali Sandstone, Anambra Basin, SE Nigeria: Implication for Its Provenance. *Comptes Rendus. Géoscience*, **342**, 136-150.  
<https://doi.org/10.1016/j.crte.2009.09.009>
- [22] Ladipo, K.O., Nwajide, C.S. and Akande, S.O. (1992) Cretaceous and Paleogene Sequences in the Abakaliki and Anambra Basins, Southeastern Nigeria: A Field Guide. International Symposium on Geology of Deltas, Port Harcourt, 39.
- [23] Reyment, R.A. (1964) Review of Nigerian Cretaceous—Cenozoic Stratigraphy. *Journal of Nigeria Mining Geological and Metallurgical Society*, **1**, 61-80.
- [24] Reyment, R.A. and Morner, N.A. (1977) Cretaceous Transgressions and Regressions Exemplified by the South Atlantic. *Paleontological Society of Japan*, **21**, 247-260.
- [25] Reyment, R.A. (1965) *Aspects of the Geology of Nigeria*. University of Ibadan Press, Ibadan, 145.
- [26] Obi, G.C. (2000) Depositional Model for the Campanian-Maastrichtian Anambra Basin, Southern Nigeria. Ph.D. Thesis, University of Nigeria, Nsukka.
- [27] Kogbe, C.A. (1989) The Cretaceous and Paleogene Sediments of Southern Nigeria. In: Kogbe, C.A., Ed., *Geology of Nigeria*, 2nd Edition, Rockview Nigeria Limited, Lagos, 273-286.
- [28] Kearey, P., Brook, S.M. and Hill, I. (2002) *Introduction to Geophysical Exploration*. Blackwell Scientific Publication, Hoboken, 272.
- [29] Telford, W.M., Geldart, L.P. and Sheriff, R.E. (1990) *Applied Geophysics*. 2nd Edition, Cambridge University Press, Cambridge.  
<https://doi.org/10.1017/CBO9781139167932>
- [30] Lowrie, W. (2007) *Fundamentals of Geophysics*. Cambridge University Press, Cambridge, 392. <https://doi.org/10.1017/CBO9780511807107>